Journal of Medicinal Chemistry

Article

pubs.acs.org/jmc

Radioiodinated Benzyloxybenzene Derivatives: A Class of Flexible Ligands Target to β-Amyloid Plaques in Alzheimer's Brains

Yanping Yang,[†] Mengchao Cui,*[,†] Xiaoyang Zhang,[†] Jiapei Dai,[‡] Zhiyong Zhang,[§] Chunping Lin,[§] Yuzhi Guo,[§] and Boli Liu[†]

[†]Key Laboratory of Radiopharmaceuticals, Ministry of Education, College of Chemistry, Beijing Normal University, Beijing 100875, P. R. China

[‡]Wuhan Institute for Neuroscience and Neuroengineering, South-Central University for Nationalities, Wuhan 430074, P. R. China

[§]Beijing ZHIBO Bio-Medical Technology Co. Ltd., Beijing 102502, P. R. China

Supporting Information

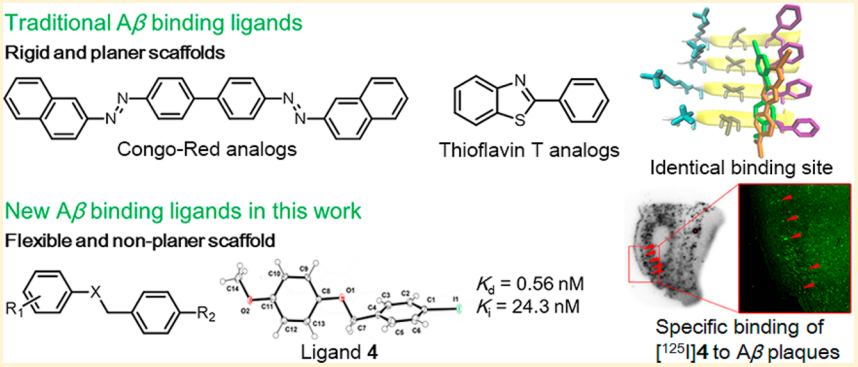

ABSTRACT: Benzyloxybenzene, as a novel flexible scaffold without rigid planarity, was synthesized and evaluated as ligand toward Aβ plaques. The binding site calculated for these flexible ligands was the hydrophobic Val18_Phe20 channel on the flat surface of Aβ fiber. Structure−activity relationship analysis generated a common trend that binding affinities declined significantly from para-substituted ligands to ortho-substituted ones, which was also quantitatively illustrated by 3D-QSAR modeling. Autoradiography in vitro further confirmed the high affinities of radioiodinated ligands [^{125}I]**4**, [^{125}I]**24**, and [^{125}I]**22** (K_i = 24.3, 49.4, and 17.6 nM, respectively). In biodistribution, [^{125}I]**4** exhibited high initial uptake and rapid washout property in the brain with $brain_{2\ min}/brain_{60\ min}$ ratio of 16.3. The excellent in vitro and in vivo biostability of [^{125}I]**4** enhanced its potential for clinical application in SPECT imaging of Aβ plaques. This approach could also allow the design of a new generation of Aβ targeting ligands without rigid and planar framework.

INTRODUCTION

As the world's population ages, we confront a looming global prevalence of Alzheimer's disease (AD), which represents a daunting, worldwide challenge for society and healthcare providers.[1] Today, the early diagnosis of AD in its preclinical phase is at the forefront of biomedical research. The amyloid cascade hypothesis, which posits that the deposition of extracellular β-amyloid (Aβ) plaques in the brain plays a causative role in the pathogeny of AD, has dominated research for the past two decades.[2] Therefore, it is of paramount clinical value to precisely detect the Aβ plaques at preclinical AD with noninvasive techniques such as positron emission tomography (PET) or single photon emission computed tomography (SPECT). It is expected to provide clues to the underlying disease pathology and aid in earlier evaluation of new disease modifying treatments.

Early diagnosis of AD has become a hot spot, with an enormous number of published studies describing in vivo or ex vivo attempts to image Aβ plaques with various radiolabeled probes. Initial inspirations toward Aβ imaging came from two categories of historic amyloid binding dyes used in neuropathology, Congo red (CR) and thioflavin T (ThT) (Figure 1). However, these dyes failed to penetrate the blood−brain barrier (BBB) because of their bulky and ionic natures.[3,4] Subsequent approaches focused on structural modifications of these dyes resulted in a great diversity of radiolabeled Aβ probes for PET or SPECT imaging. The chemical scaffolds derived from ThT including benzothiazole,[5,6] benzoxazole,[7] benzothiophene,[8] benzofuran,[9] imidazopyridine,[10] benzoimidazole,[11] and so on. Stilbene[12,13] and its analogues such as biphenyl,[14] biphenylalkyne,[15] and diphenyl-1,3,4-oxadiazole[16] were also well studied. In addition, another series of frameworks generated from plant pigments like curcumin,[17] flavone,[18] chalcone,[19] and aurone[20] were radiolabeled and biologically investigated. Among them, several PET imaging agents targeting to Aβ plaques have

Received: March 20, 2014

   dx.doi.org/10.1021/jm5004396 | J. Med. Chem. XXXX, XXX, XXX−XXX

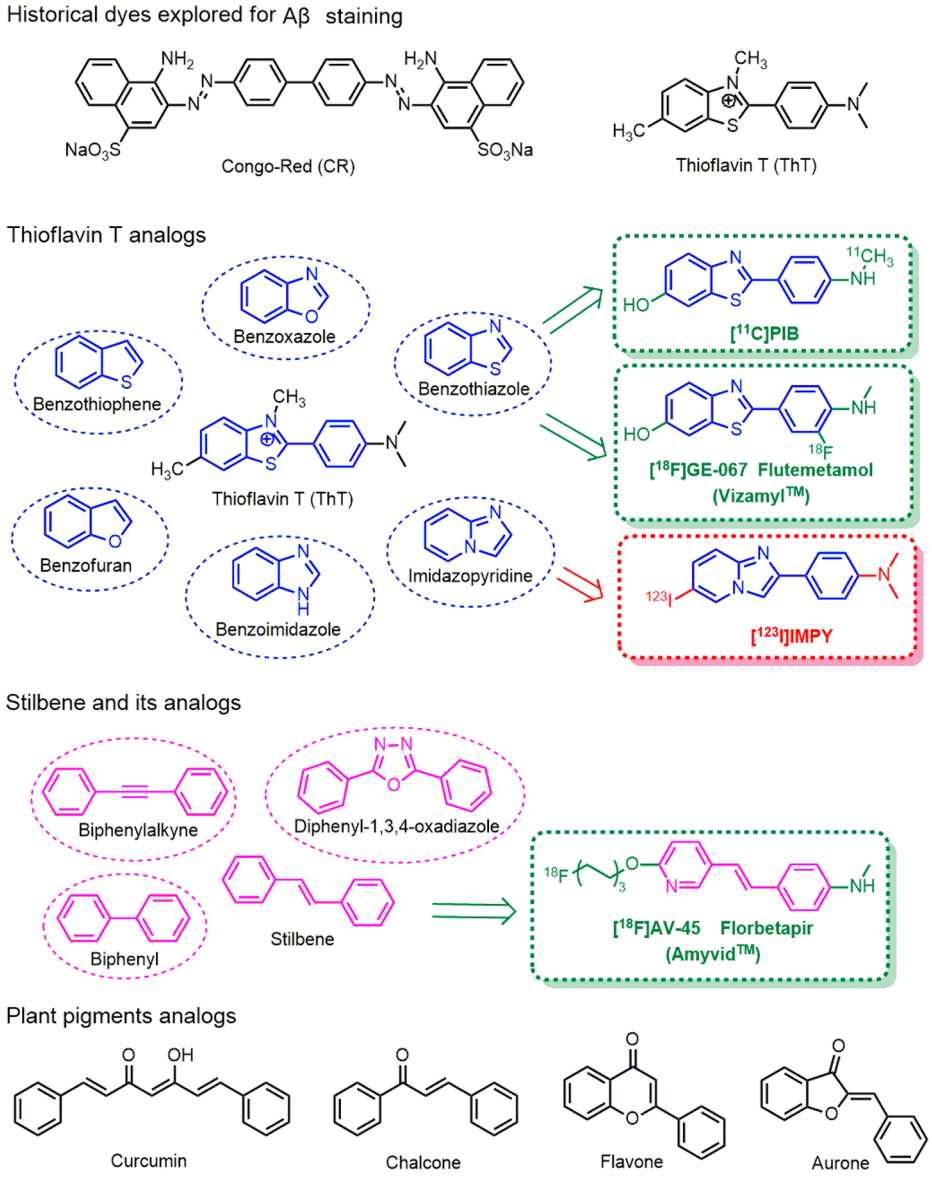

Figure 1. Chemical structures of dyes originally utilized for Aβ staining and scaffolds explored for PET/SPECT imaging of Aβ plaques in AD patients.

achieved wonderful progress. [^{11}C]PIB[5] has been studied in human from 2002, and almost 10000 PET scans have been conducted worldwide. Better yet, [^{18}F]AV-45 (florbetapir),[13,21] [^{18}F]GE-067 (flutemetamol),[6] and [^{18}F]BAY94-9172 (florbetaben)[22] have been approved by the U.S. FDA in the last two years. In contrast, the approach in developing a selective SPECT agent to quantify Aβ plaques in living human brain has intensively lagged behind. Preliminary clinical data of [^{123}I]IMPY (Figure 1), the only SPECT tracer tested in humans, showed excellent binding property, high brain penetration, and fast washout kinetics.[10] Unfortunately, its signal-to-noise ratio for plaque labeling was not robust in AD and normal subjects, thus preventing its translation to clinical use. The in vivo instability and rapid metabolism were deemed as main causes of the low contrast and poor image quality.[23]

From the foregoing overview of these Aβ binding probes, we can easily draw a conclusion that the chemical diversity of their scaffolds has been confined to small variations of the traditional dyes.[24] Most, if not all, of them contain two aromatic moieties and retain the highly rigid and planar scaffold with π-conjugated systems, which are widely believed as vital points of the specific binding between probes and Aβ fibers.[25] This common feature gave strong impulse to our bold attempts to break the conjugated backbone and make "out of box" innovation. Herein, we describe the preliminary characterization of a series of benzyloxybenzene derivatives without highly conjugated structure to screen novel Aβ probes with favorable binding affinities and brain pharmacokinetics. This study could probably expand the chemical library of Aβ probes and provide more impetus for designing novel tracers off from the traditional thought pattern that the conjugated and planar framework is essential. Computational simulations including three-dimensional quantitative structure–activity relationship (3D-QSAR) modeling and molecular docking were also carried out to further clarify the interaction mechanism between benzyloxybenzene derivatives and Aβ fibers.

RESULTS AND DISCUSSION

Chemistry. The synthesis of the benzyloxybenzene derivatives is outlined in Scheme 1. Twenty-two iodinated ligands and three tributyltin precursors were successfully produced with

dx.doi.org/10.1021/jm5004396 | J. Med. Chem. XXXX, XXX, XXX−XXX

Scheme 1[a]

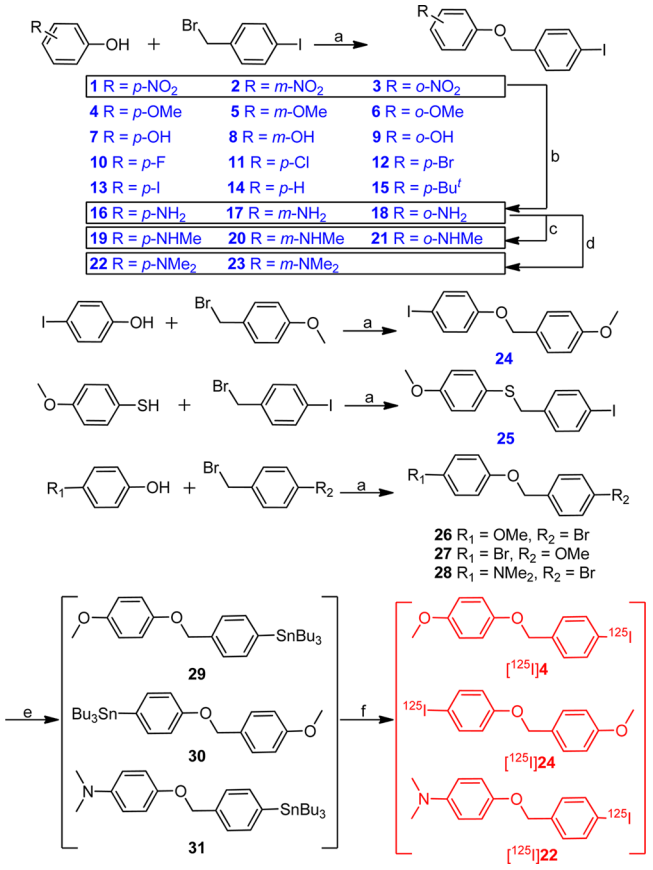

[a]Reagents and conditions: (a) K_2CO_3, DMF, 90 °C; (b) $SnCl_2 \cdot 2H_2O$, EtOH, HCl, reflux; (c) (1) NaOMe, $(CH_2O)_n$, MeOH, reflux, (2) $NaBH_4$, reflux; (d) $(CH_2O)_n$, $NaBH_3CN$, HAc, rt; (e) $(Bu_3Sn)_2$, $(PPh_3)_4Pd$, toluene, Et_3N, reflux; (f) [^{125}I]NaI, HCl (1 M), H_2O_2 (3%).

common methods and verified with $^1H/^{13}C$ NMR and MS (EI). Purities of key compounds were proved to be higher than 98% by high-performance liquid chromatography (HPLC).

Structure–Activity Relationships. As analyzed above, almost all the previously reported Aβ probes were flat molecules. The crystal of stilbene scaffold, one of the most studied scaffolds for developing Aβ imaging agents, visually confirmed its rigid and flat natures (Supporting Information Figure S1e). To illustrate the molecular geometries of the novel benzyloxybenzene scaffold, single crystals of compound **4** and **6** were elucidated, and the crystallographic data were summarized in Supporting Information Table S1. As expected, differing significantly from stilbene and other π-conjugated backbones for Aβ imaging, their structures were more flexible and the two phenyl rings were not coplanar any more with the dihedral angles up to 60.02° and 74.81°, respectively (Supporting Information Figure S1). To evaluate the binding affinities of these different benzyloxybenzene ligands to $A\beta_{42}$ aggregates, saturation binding experiment of [^{125}I]**4** was first conducted and the K_d value was calculated to be 0.56 ± 0.18 nM (Supporting Information Figure S2). Afterward, competition binding assay of established reference ligands IMPY and PIB was performed using [^{125}I]**4** as the competing radioligand. To our surprise, IMPY and PIB both displayed comparable affinities (K_i = 32.2 ± 2.1; 38.8 ± 2.6 nM) which indicated that IMPY and PIB competed well against [^{125}I]**4** (Table 1). These results indicated that benzyloxybenzene derivatives shared the same binding site with IMPY and PIB, the thioflavin binding site. Binding affinities of iodinated benzyloxybenzene ligands were evaluated by competition binding assay under identical test conditions. The data in Table 1 distinctly suggested that the substituents' position, para/meta/ortho, on the phenyl ring exhibited astonishing influence on binding property toward Aβ aggregates. A common regularity was obviously discovered that the binding affinities decreased dramatically from para-position to ortho-position (substituent OMe, **4** > **5** > **6**; OH, **7** > **8** > **9**; NHMe, **19** > **20** > **21**; NMe_2, **22** > **23**). Notably, ligand **4**, with a *p*-OMe substituent, showed about 5-fold higher affinity than **5** with *m*-OMe, 210-fold higher than **6** with *o*-OMe, similarly, ligand **19** with *p*-NHMe displayed about 12-fold higher affinity than **20** with *m*-NHMe and 438-fold higher than **21** with *o*-NHMe. When considering the substituents, the slight decline in binding affinity was observed from *N*,*N*-dimethylamino, methoxy, *N*-monomethylamino, hydroxyl to amino group. Benzyloxybenzene with *p*-F, *p*-H, and *p*-Bu^t substituents displayed moderate affinities, with K_i values around 100 nM. Introducing halogen Cl, Br, and I at the para position staggeringly improved the binding affinities to a degree mildly better than well-known IMPY and PIB (**11**, K_i = 18.8 ± 2.2 nM; **12**, K_i = 12.0 ± 1.0 nM; **13**, K_i = 21.9 ± 2.1 nM). When changing the position of iodine atom to the opposite side of the molecule, K_i value increased from 24.3 nM of **4** to 49.4 nM of **24**. Replacing oxygen in the core with its bioisostere, sulfur, resulted in strong decline in binding affinity (**25**, K_i = 530.2 nM).

To quantitatively illustrate the structure–activity correlation of benzyloxybenzene derivatives, 3D-QSAR modeling was performed. Twenty-one benzyloxybenzene molecules and IMPY were first geometry optimized at the B3LYP/6-31G and 3-21G level in the water phase. The optimized structures of compound **4** and **6** conformed well to the geometries of their X-ray crystals in root-mean-square deviations (RMSD) of 0.20 and 0.07 Å, respectively. The small RMSD values guaranteed the credibility of using the optimized structures for the QSAR and molecular docking calculations. 3D-QSAR studies successfully yielded two statistically reliable models, including comparative molecular field analysis (CoMFA: r^2, 0.947; q^2, 0.606) and comparative molecular similarity indices analysis (CoMSIA: r^2, 0.988; q^2, 0.777), which were able to predict binding abilities of novel derivatives accurately. CoMFA and CoMSIA analysis results were summarized in Figure 2c, and it showed that the electrostatic field with the highest contributions (53.4% in CoMFA; 38.2% in CoMSIA) was the dominant factor for Aβ binding affinities. The actual and predicted pK_i values obtained from CoMFA and CoMSIA models were graphed in parts d and e of Figure 2, respectively. Ideally, all of the data points appeared on or close to the diagonal, which sufficiently demonstrated that the calculated pK_i were in good agreement with the experimental data. The deviations of the calculated pK_i values from the corresponding actual data in both models were all smaller than 0.5 log unit. To graphically visualize the CoMFA/CoMSIA results, the steric, electrostatic, hydrophobic, hydrogen-bond donor, and hydrogen-bond acceptor fields were aligned with the conformation of ligand **4** and presented as 3D coefficient contour plots in Figure 2f–i. The CoMFA steric contours (Figure 2f) show a favored green area at the para-position of the phenyl ring indicating that the bulky substituents are desirable. All the ortho-substituted ligands (**6**, **9**, **18**, and **21**), which displayed shocking degradation of binding affinities, exhibited significant encroachment in the disfavored yellow contours. In Figure 2g, the blue counter around the para-position and a small blue region near the ortho-position suggest that more positively charged substituents at the position

dx.doi.org/10.1021/jm5004396 | J. Med. Chem. XXXX, XXX, XXX–XXX

Table 1. Inhibition Constants for the Binding of [^{125}I]4 to Aβ_{42} Aggregates[a]

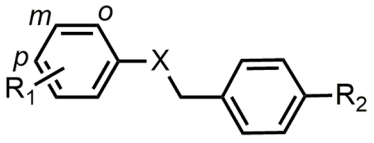

Scaffold

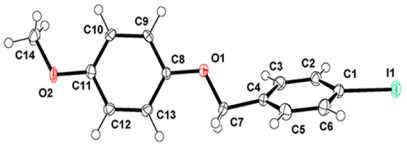

Crystal Structure of 4

compd	R_1	X	R_2	K_i (nM)	pK_i
4	*p*-OMe	O	I	24.3 ± 6.8	7.61
5	*m*-OMe	O	I	130.6 ± 4.8	6.88
6	*o*-OMe	O	I	5164.8 ± 410.3	5.29
7	*p*-OH	O	I	113.4 ± 23.8	6.95
8	*m*-OH	O	I	385.6 ± 114.2	6.41
9	*o*-OH	O	I	2831.2 ± 517.0	5.55
10	*p*-F	O	I	107.1 ± 15.4	6.97
11	*p*-Cl	O	I	18.8 ± 2.2	7.73
12	*p*-Br	O	I	12.0 ± 1.0	7.92
13	*p*-I	O	I	21.9 ± 2.1	7.66
14	*p*-H	O	I	79.4 ± 5.2	7.10
15	*p*-Bu^t	O	I	117.6 ± 17.7	6.93
16	*p*-NH_2	O	I	409.2 ± 45.0	6.39
17	*m*-NH_2	O	I	1534.7 ± 159.7	5.81
18	*o*-NH_2	O	I	1028.0 ± 49.0	5.99
19	*p*-NHMe	O	I	48.2 ± 4.3	7.32
20	*m*-NHMe	O	I	593.6 ± 78.2	6.23
21	*o*-NHMe	O	I	20662 ± 2653	4.68
22	*p*-NMe_2	O	I	17.6 ± 1.6	7.75
23	*m*-NMe_2	O	I	894.2 ± 88.0	6.05
24	I	O	OMe	49.4 ± 3.0	7.31
25	*p*-OMe	S	I	530.2 ± 109.4	6.28
IMPY				32.2 ± 2.1	7.49
PIB				38.8 ± 2.6	7.41

[a]Measured in triplicate with values given as the mean ± SD.

may enhance the binding abilities. On the contrary, two red areas illustrate that more negatively charged groups are favorable at that position. A yellow-colored polyhedron close to the para-position (Figure 2h) indicates that adding hydrophobic substituents will be propitious to improve binding affinities. Three large white polyhedrons represent regions where decreased hydrophobic interaction is helpful in increasing binding abilities. In Figure 2i, large cyan regions represent areas where hydrogen-bond donor groups on the ligand are predicted to enhance binding, while the purple area is predicted to disfavor binding. A small region in red was hydrogen-bond acceptors unfavorable. All the structural insights acquired from 3D-QSAR contour maps were in coincidence with the experimental affinity data and reasonably instructive for future drug design.

Molecular Docking. To further understand the binding nature of these novel benzyloxybenzene ligands to Aβ fiber, docking simulations were also carried out. Several previously reported articles, which investigated molecular interactions of Aβ binding ligands with fiber, revealed that the hydrophobic cleft formed between Val18 and Phe20 was the most probable and feasible binding site.[26] Thus, resides 16-KLVFFA-21 on the surface of Aβ fiber (PDB 2LMO) were selected for docking with grids centered on this region. Computational docking results revealed that all the benzyloxybenzene analogues, similar to IMPY, inserted into the hydrophobic Val18_Phe20 channel with long molecular axes oriented longitudinally to the fiber axis (Figure 3a–c). This observation sufficiently verified the results from inhibition binding assay that benzyloxybenzene ligands shared the same binding site with IMPY. Analyzing the binding energy (ΔG) of top-ranking conformations for each analogue gained a qualitative linear correction with experimental pK_i in high R^2 value of 0.875 (Figure 3d). After packing into the binding patch, all the flexible benzyloxybenzene analogues with substituents at the para-position tended to be locked into a near-flat conformation. For instance, the dihedral angle between the two phenyl planes in ligand **4** decreased from 60.02° to 40.40° after docking. The near-flat characteristic of these ligands favored their impaction into the hydrophobic channel with low binding energies, which exactly justified their high binding affinities. On the contrary, ligand **6** and **21** with ortho-substituents held greater degrees of nonplanarity in the top-ranking poses and were harder to be accommodated in the shallow binding channel, correspondingly resulting in high binding energies and low binding affinities fit the binding pocket. This binding mode generated by docking simulations was in good agreement with the experimental data and 3D-QSAR models.

Radiochemistry. Iodinated ligands **4** and **22** with high binding affinities were selected for radiolabeling and further biological evaluations. To evaluate the impact of iodine's position on biological properties, ligand **24** with iodine atom on the opposite side of the backbone was also pitched on. Radiochemical synthesis of [^{125}I]**4**, [^{125}I]**24**, and [^{125}I]**22** was reproducibly achieved via an iododestannylation reaction in high radiochemical yields of 86.2%, 94.9%, and 92.9%, respectively. After purification by

dx.doi.org/10.1021/jm5004396 | J. Med. Chem. XXXX, XXX, XXX–XXX

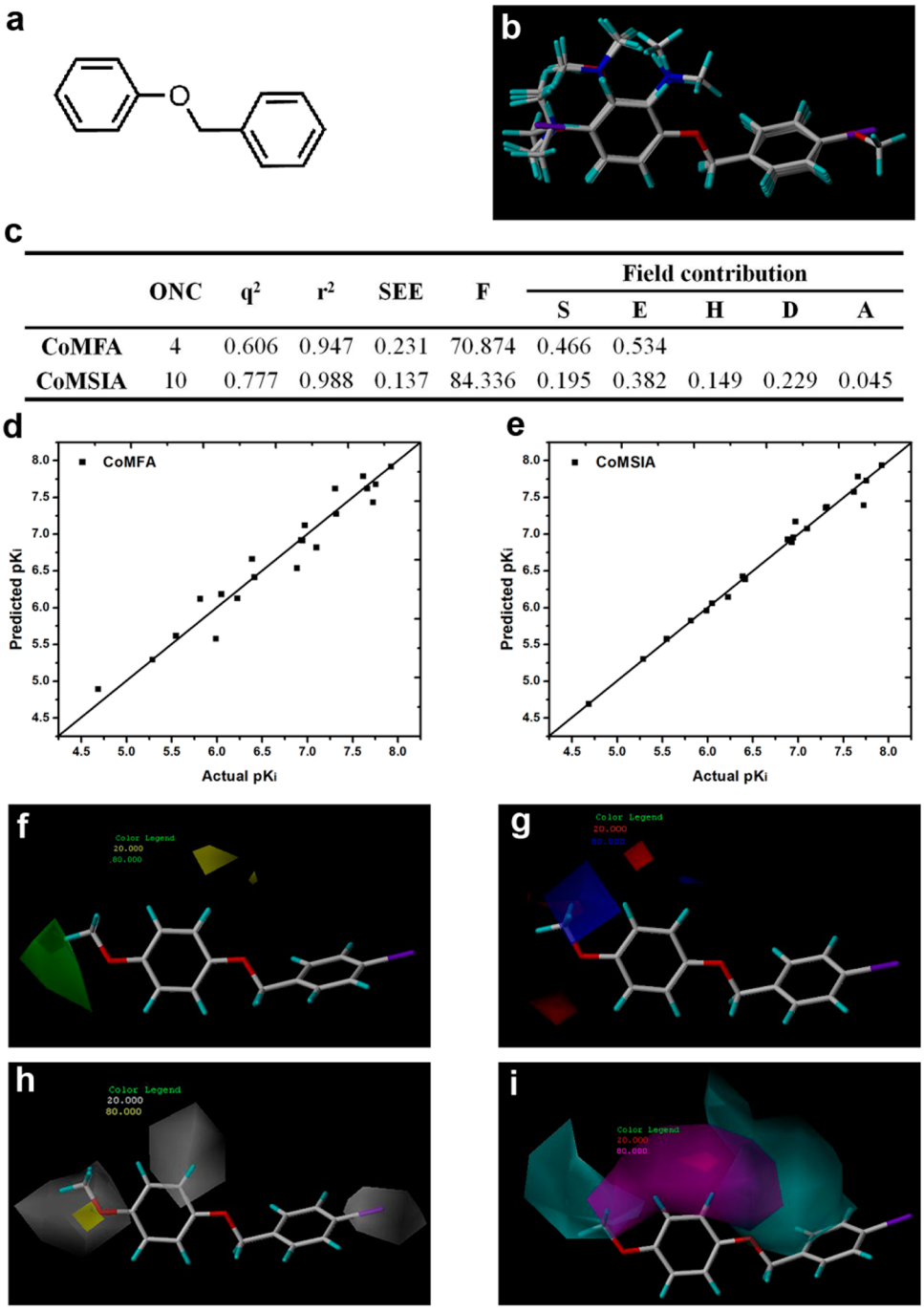

	ONC	q^2	r^2	SEE	F	Field contribution				
						S	E	H	D	A
CoMFA	4	0.606	0.947	0.231	70.874	0.466	0.534			
CoMSIA	10	0.777	0.988	0.137	84.336	0.195	0.382	0.149	0.229	0.045

Figure 2. Construction of good predictive CoMFA and CoMSIA 3D-QSAR models. (a) Common core selected for database alignment. (b) Superposition of compounds **4**–**24**. (c) Statistical parameters of CoMFA and CoMSIA models. ONC: optimum number of components. q^2: leave one out (LOO) cross-validated correlation coefficient. r^2: nonvalidated correlation coefficient. SEE: standard error of estimate. F: *F*-test value. S, E, H, D, A: relative contributions of steric, electrostatic, hydrophobic, and hydrogen-bond donor and acceptor fields, respectively. (d,e) Correlation between actual and predicted pK_i of 3D-QSAR models (d, CoMFA model; e, CoMSIA model). (f–i) Contour maps of CoMFA (f,g) and CoMSIA (h,i) models. Scattered green areas are sterically favored, yellow areas are unfavorable. Red regions are negative potential favored, while blue areas are unfavorable. Yellow areas are regions where hydrophobic groups are desirable, white areas are undesirable. Large cyan regions represent areas where hydrogen donors on the ligand are predicted to enhance binding, while purple areas are predicted to disfavor binding. Regions in magenta are hydrogen acceptor favored, and regions in red are unfavorable. The most promising compound **4** was superposed as the reference molecule in these maps. These contour maps generated depict regions with scaled coefficients greater than 80% (favored) or less than 20% (disfavored).

HPLC, the radiochemical purity of these radiotracers was higher than 95%. The radiochemical identities of ^{125}I-labeled tracers were verified by comparison of the retention times with that of the nonradioactive compounds (Supporting Information Table S2, Figure S3).

In Vitro Autoradiography. We further confirmed the specific binding of [^{125}I]**4**, [^{125}I]**24**, and [^{125}I]**22** to Aβ plaques with in vitro autoradiography on brain sections from AD patients and Tg model mice. As shown in Figure 4, marked labeling of Aβ plaques was observed on sections of AD patients and Tg mice

dx.doi.org/10.1021/jm5004396 | J. Med. Chem. XXXX, XXX, XXX–XXX

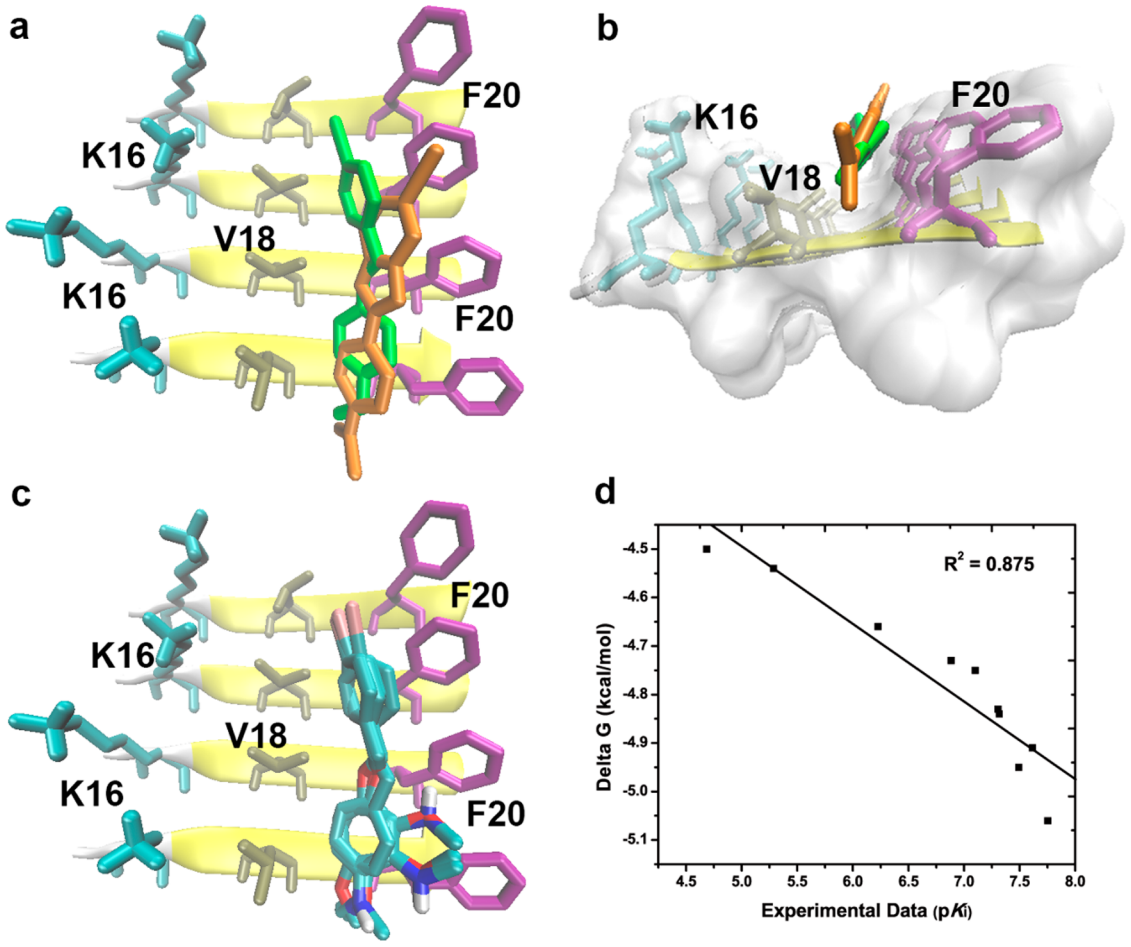

Figure 3. Computational docking models of IMPY and benzyloxybenzene analogues on Aβ fiber. (a) IMPY and ligand **4** bound along the hydrophobic grooves formed between Val18 and Phe20 running longitudinally to the long axis of the β-sheet. (b) Identical binding model viewed down the fiber axis with molecular surface of the protein represented by transparent material. (c) Lowest energy docked conformations of nine benzyloxybenzene derivatives. (d) ΔG correlated well with experimental pK_i in reasonably high R^2 value of 0.875.

brain, and the location of accumulated radioactivity was in conformity with the position of Aβ plaques stained with thioflavin-S, a conventional dye usually used for plaque staining (Figure 4a,e,i and c,g,k), while the healthy human and wild-type mice brain showed no such concentration of radioactivity (Figure 4b,f,j and d,h,l).

In Vivo Biodistribution. To assess BBB penetration and washout properties of [^{125}I]**4**, [^{125}I]**24**, and [^{125}I]**22**, partition coefficient determination and biodistribution assays in normal ICR mice were implemented. The log *D* values determined for [^{125}I]**4**, [^{125}I]**24**, and [^{125}I]**22** were 4.00 ± 0.08, 4.16 ± 0.29, and 2.89 ± 0.09, respectively, indicating that the three ^{125}I-labeled tracers have appropriate lipophilicity to penetrate BBB (Supporting Information Table S3). As shown in Figure 5, all the three ^{125}I-labeled ligands exhibited high initial brain uptakes (>4%ID/g at 2 min postinjection) and rapid washout rates from healthy brain (<0.5%ID/g at 60 min postinjection). Most of all, [^{125}I]**4** provided the highest brain uptake with 6.18%ID/g at 2 min and fast clearance from normal brain with $\text{brain}_{2\ \text{min}}$/$\text{brain}_{60\ \text{min}}$ ratio of 16.3, which were superior to the results of [^{125}I]IMPY gained under the same procedure. Moreover, [^{125}I]IMPY displayed slender deiodination, while no increase of accumulated radioactivity in thyroids was observed over time in the biodistribution experiment of [^{125}I]**4**. The excellent pharmacokinetics of the three ^{125}I labeled ligands strongly demonstrated that the novel chemical scaffold was qualified for imaging Aβ plaques in the brain, and [^{125}I]**4** with optimal properties was selected for further investigation.

In Vitro Biostability of [^{125}I]4. When incubated in mouse plasma at 37 °C, [^{125}I]IMPY underwent severe chemical degradation (Supporting Information Figure S4c). At 60 min, only half of radioactivity remained as parent tracer and three other metabolized radioactive substances with shorter retention times were detected. Conversely, [^{125}I]**4** displayed excellent in vitro biostability when incubated in mouse plasma and liver homogenate under the same condition with 100% of radioactivity existed as the intact form (Supporting Information Figures S4a, 4b). The in vitro experiments in both plasma and liver homogenate sufficiently demonstrated high biostability of [^{125}I]**4**, which is an indispensable criterion for drug delivery.

In Vivo Biostability of [^{125}I]4. The in vivo metabolic stability of [^{125}I]**4** was evaluated by HPLC analysis of each organ sample of normal ICR mice obtained at different postinjection time points (Figure 6). Two polar radioactive metabolites were detected. In brain, only one metabolic product, metabolite 2, was observed. The percentage of the parent tracer was 95.0% at 2 min, and almost 40% of the radioactivity remained to be the intact form at 60 min. In plasma, the fraction of unchanged [^{125}I]**4** decreased rapidly from 71.5% at 2 min to 10.6% at 60 min, whereas the major metabolite 1 increased to 85.3% at 60 min.

dx.doi.org/10.1021/jm5004396 | J. Med. Chem. XXXX, XXX, XXX−XXX

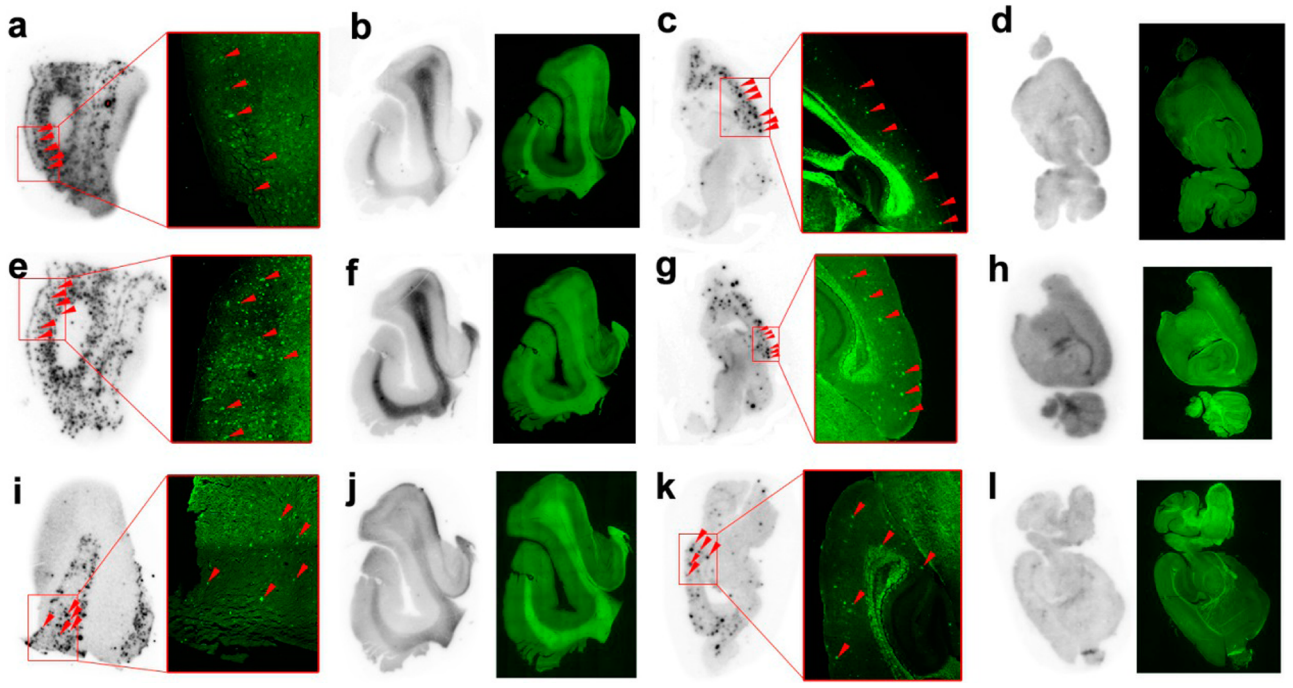

Figure 4. autoradiography of [^{125}I]**4**, [^{125}I]**24**, and [^{125}I]**22** in human brain sections ((a,e,i) AD, 64 years old, female; (b,f,j) normal, 74 years old, male) and mouse brain sections ((c,g,k) Tg mouse, APPswe/PSEN1, 11 months old; (d,h,l) wild-type, C57BL6, 11 months old). The presence and distribution of plaques in the sections were confirmed with thioflavin-S.

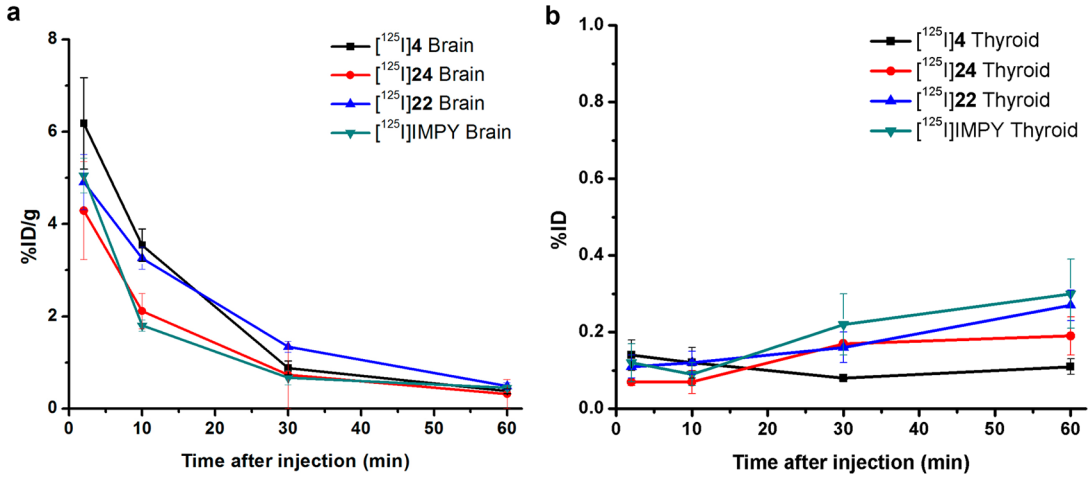

Figure 5. Comparison of brain and thyroid uptake of [^{125}I]**4**, [^{125}I]**24**, [^{125}I]**22**, and [^{125}I]IMPY in normal ICR mice.

A small amount of metabolite 2 was also found in plasma. In the liver at 2 min, 42.4% parent tracer was presented and the rest radioactivity was partitioned 42.9% as metabolite 1 and 14.7% as metabolite 2. From 30 to 60 min, almost no parent tracer was discovered, and the radioactivity presented mainly as metabolite 1. In urine samples, radioactivity was detected only after 10 min and more than three-quarters existed as metabolite 1. Compared with other tissues, the amount of radioactivity in feces was too low to be detected by HPLC. This preliminary metabolism study illustrated that [^{125}I]**4** was converted to two radiochemical forms. Metabolite 2 was predominately generated in brain, while metabolite 1 was mainly yielded in liver and cannot cross the BBB.

CONCLUSION

Different from the conventional Aβ binding ligands, a novel flexible scaffold, benzyloxybenzene, without the big π-conjugated system and rigid planarity, was discovered. Amazingly, benzyloxybenzene derivatives competed well against IMPY and exhibited various binding affinities to Aβ_{42} aggregates, with K_i values differing from 12.0 nM to larger than 20000 nM. Molecular docking successfully determined that this series of flexible ligands and IMPY shared the same hydrophobic Val18_Phe20 channel on the flat spine of Aβ fiber. Together with 3D-QSAR studies, structure−activity relationships were clarified. Severe decline in binding affinities was found from para-substituted ligands to ortho-substituted ones. Subsequently, [^{125}I]**4**, [^{125}I]**24**, and [^{125}I]**22** with high binding affinities (K_i = 24.3, 49.4, and 17.6 nM, respectively) were reproducibly synthesized in radiochemical yields higher than 85%. Autoradiography in vitro showed that the ^{125}I-labeled ligands specifically labeled Aβ plaques on sections of AD patients and Tg mice brain. In biodistribution, the ^{125}I-labeled ligands displayed excellent in vivo

dx.doi.org/10.1021/jm5004396 | J. Med. Chem. XXXX, XXX, XXX−XXX

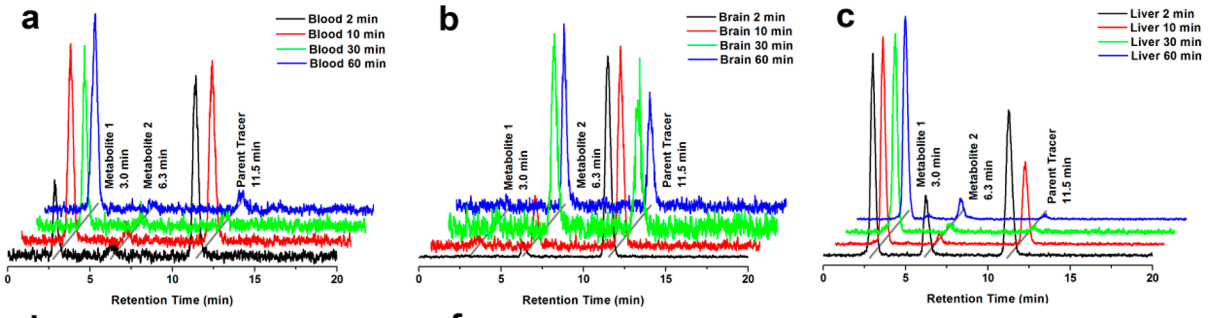

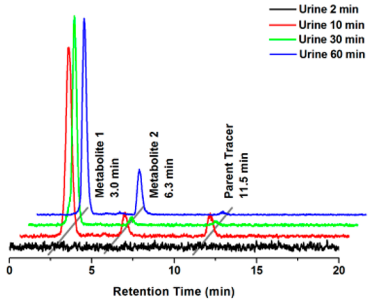

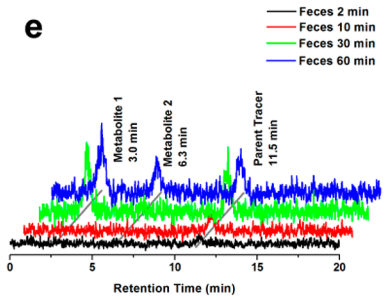

f

Organ	Time (min)	Metabolite 1	Metabolite 2	Parent tracer
Brain	2	-	5.0%	95.0%
	10	-	18.0%	82.0%
	30	-	53.4%	46.6%
	60	-	61.1%	38.9%
Blood	2	22.3%	6.2%	71.5%
	10	45.9%	4.4%	49.7%
	30	79.0%	2.8%	18.2%
	60	85.3%	4.2%	10.6%
Liver	2	42.9%	14.7%	42.4%
	10	64.7%	3.5%	31.9%
	30	90.3%	7.2%	2.5%
	60	85.3%	10.8%	1.9%
Urine	2	-	-	-
	10	83.7%	7.9%	8.4%
	30	94.5%	3.2%	2.4%
	60	78.8%	19.9%	1.3%
Feces	2	-	-	-
	10	-	-	100%
	30	50.1%	-	49.9%
	60	38.0%	21.4%	40.6%

Figure 6. HPLC profiles for in vivo biostabilities of [^{125}I]**4** in ICR mice blood (a), brain (b), liver (c), urine (d), and feces (e). (f) Percentages of the parent tracer, metabolite 1 and metabolite 2 in each organ at 2, 10, 30, and 60 min time points. HPLC conditions: Venusil MP C18 column (Agela Technologies, 5 μm, 4.6 mm × 250 mm), CH_3CN/H_2O = 80%/20%, 1 mL/min.

pharmacokinetics. Especially, [^{125}I]**4** exhibited the highest brain uptake with 6.18%ID/g at 2 min postinjection and rapid clearance property with $brain_{2\ min}/brain_{60\ min}$ ratio of 16.3. Contrary to IMPY, no deiodination of [^{125}I]**4** was observed. More importantly, [^{125}I]**4** displayed good in vitro biostability in mouse plasma and liver homogenate (100% intact form at 60 min) and considerably overcame the instability of [^{125}I]IMPY, which was a limiting factor for its clinical use. In metabolism studies, two polar radioactive metabolites of [^{125}I]**4** were detected. In the brain, [^{125}I]**4** showed agreeable in vivo biostability with almost 40% of the radioactivity remained to be the parent tracer until 60 min.

In conclusion, this innovative finding could offer new insights for imaging of Aβ plaques in Alzheimer's brains. The rigid and planar scaffold with big π-conjugated system was not indispensable for Aβ probes, and the binding pocket of Aβ fiber exhibited considerable tolerance to a certain degree of distortion of small molecule ligands. This would provide new hints for developing Aβ targeting ligands with flexible framework to enable improved localization and quantitative imaging of Aβ plaques. In addition, we believe that [^{125}I]**4** with optimal qualities could potentially be translated into clinical practice for SPECT imaging of Aβ plaques in AD brains.

EXPERIMENTAL SECTION

General Remarks. All reagents used for chemical synthesis were commercial products and were used without further purification. [^{125}I]NaI was purchased from PerkinElmer. ^{1}H NMR (400 MHz) and ^{13}C NMR (100 MHz) spectra were acquired on Bruker Avance III NMR spectrometers in $CDCl_3$ or DMSO-d_6 solutions at room temperature with trimethylsilyl (TMS) as an internal standard. Mass spectra were acquired with a GCT CA127 Micronass UK instrument. X-ray crystallography data were collected on a Bruker Smart APEX II diffractometer (Bruker Co., Germany). HPLC was performed on a Shimadzu SCL-20 AVP (which was equipped with a Bioscan Flow Count 3200 NaI/PMT γ-radiation scintillation detector and a SPD-20A UV detector, λ = 254 nm) and a Venusil MP C18 reverse phase column (Agela Technologies, 5 μm, 4.6 mm × 250 mm) eluted with a binary gradient system (acetonitrile:water = 80:20%) at a 1.0 mL/min flow rate. Fluorescent observation was performed on the Axio Observer Z1 inverted fluorescence microscope (Zeiss, Germany) equipped with a DAPI filter set (excitation, 405 nm). Normal ICR mice (5 weeks, male) were used for biodistribution experiments. Human brain sections of an autopsy-confirmed AD (64 years old, female), and a control subject (74 years old, male) were obtained from Chinese Brain Bank Center. Transgenic mice (APPswe/PSEN1, male, 11 months old) and wild-type mice (C57BL6, male, 11 months old) were purchased from the Institute of Laboratory Animal Science, Chinese Academy of Medical Sciences.

dx.doi.org/10.1021/jm5004396 | J. Med. Chem. XXXX, XXX, XXX−XXX

All protocols requiring the use of mice were approved by the animal care committee of Beijing Normal University.

*1-Iodo-4-((4-nitrophenoxy)methyl)benzene (**1**).* To a solution of 4-nitrophenol (695.6 mg, 5.0 mmol) and 1-(bromomethyl)-4-iodobenzene (1.48 g, 5.0 mmol) in anhydrous DMF (5 mL) was added K_2CO_3 (1.38 g, 10.0 mmol). The resulting mixture was stirred at 90 °C for 2 h; after cooling to room temperature, 50 mL of water was added and a white precipitate was formed. The precipitate was collected by filtration, washed with 50 mL of water, and recrystallized from methanol to give **1** as a white solid (1.69 g, 95.2%). HPLC: 7.51 min, 99.8%; mp 147.4–148.1 °C. ^{1}H NMR (400 MHz, $CDCl_3$) δ 8.21 (d, J = 9.2 Hz, 2H), 7.75 (d, J = 8.3 Hz, 2H), 7.18 (d, J = 8.3 Hz, 2H), 7.01 (d, J = 9.2 Hz, 2H), 5.10 (s, 2H). ^{13}C NMR (101 MHz, $CDCl_3$) δ 163.37, 141.85, 137.91, 135.19, 129.24, 125.94, 114.84, 94.10, 69.97. MS (EI): m/z calcd for $C_{13}H_{10}INO_3$ 355; found 355 M^+.

*1-(4-Iodobenzyloxy)-3-nitrobenzene (**2**).* The procedure described above for the preparation of **1** was employed to afford **2** as a white solid (345.5 mg, 97.3%). HPLC: 8.53 min, 99.9%; mp 75.2–75.9 °C. ^{1}H NMR (400 MHz, $CDCl_3$) δ 7.85 (d, J = 8.0 Hz, 1H), 7.80 (s, 1H), 7.74 (d, J = 8.2 Hz, 2H), 7.45 (t, J = 8.2 Hz, 1H), 7.30–7.26 (m, 1H), 7.19 (d, J = 8.1 Hz, 2H), 5.09 (s, 2H). ^{13}C NMR (101 MHz, $CDCl_3$) δ 158.91, 149.19, 137.84, 135.41, 130.06, 129.29, 121.84, 116.18, 109.21, 93.99, 69.88. MS (EI): m/z calcd for $C_{13}H_{10}INO_3$ 355; found 355 M^+.

*1-(4-Iodobenzyloxy)-2-nitrobenzene (**3**).* The procedure described above for the preparation of **1** was employed to afford **3** as a yellow solid (238.9 mg, 67.3%). HPLC: 6.03 min, 99.5%; mp 70.6–71.5 °C. ^{1}H NMR (400 MHz, $CDCl_3$) δ 7.87 (dd, J = 8.1, 1.4 Hz, 1H), 7.73 (d, J = 8.2 Hz, 2H), 7.56–7.46 (m, 1H), 7.22 (d, J = 8.1 Hz, 2H), 7.09–7.04 (m, 2H), 5.18 (s, 2H). ^{13}C NMR (101 MHz, $CDCl_3$) δ 151.62, 140.23, 137.80, 135.27, 134.07, 128.78, 125.73, 120.90, 115.03, 93.80, 70.45.

*1-Iodo-4-((4-methoxyphenoxy)methyl)benzene (**4**).* The procedure described above for the preparation of **1** was employed to afford **4** as a white solid (255.3 mg, 75.1%). HPLC: 8.28 min, 99.5%; mp 128.9–130.2 °C. ^{1}H NMR (400 MHz, $CDCl_3$) δ 7.71 (d, J = 8.2 Hz, 2H), 7.17 (d, J = 8.2 Hz, 2H), 6.89 (d, J = 9.2 Hz, 2H), 6.83 (d, J = 9.2 Hz, 2H), 4.96 (s, 2H), 3.77 (s, 3H). ^{13}C NMR (101 MHz, $CDCl_3$) δ 154.18, 152.68, 137.63, 137.08, 129.25, 115.92, 114.72, 93.30, 70.07, 55.72. HRMS (EI): m/z calcd for $C_{14}H_{13}IO_2$ 339.9960; found 339.9966 M^+.

*1-(4-Iodobenzyloxy)-3-methoxybenzene (**5**).* The procedure described above for the preparation of **1** was employed to afford **5** as a white solid (211.7 mg, 62.2%). HPLC: 8.68 min, 98.5%; mp 77.4–78.7 °C. ^{1}H NMR (400 MHz, $CDCl_3$) δ 7.71 (d, J = 8.1 Hz, 2H), 7.21–7.17 (m, 3H), 6.57–6.50 (m, 2H), 4.99 (s, 2H), 3.79 (s, 3H). ^{13}C NMR (101 MHz, $CDCl_3$) δ 160.87, 159.75, 137.65, 136.71, 129.94, 129.26, 106.93, 106.73, 101.44, 93.42, 69.30, 55.27. MS (EI): m/z calcd for $C_{14}H_{13}IO_2$ 340; found 340 M^+.

*1-(4-Iodobenzyloxy)-2-methoxybenzene (**6**).* The procedure described above for the preparation of **1** was employed to afford **6** as a white solid (288.1 mg, 84.7%). HPLC: 6.63 min, 98.7%; mp 110.4–110.8 °C. ^{1}H NMR (400 MHz, $CDCl_3$) δ 7.69 (d, J = 8.1 Hz, 2H), 7.19 (d, J = 8.0 Hz, 2H), 6.97–6.91 (m, 2H), 6.85 (d, J = 3.8 Hz, 2H), 5.10 (s, 2H), 3.89 (s, 3H). ^{13}C NMR (101 MHz, $CDCl_3$) δ 149.78, 147.89, 137.58, 137.00, 129.11, 121.76, 120.78, 114.41, 112.03, 93.25, 70.41, 55.92. MS (EI): m/z calcd for $C_{14}H_{13}IO_2$ 340; found 340 M^+.

*4-(4-Iodobenzyloxy)phenol (**7**).* To a solution of hydroquinone (110.1 mg, 1.0 mmol) and 1-(bromomethyl)-4-iodobenzene (296.9 mg, 1.0 mmol) in anhydrous DMF (5 mL) was added K_2CO_3 (276.4 mg, 2.0 mmol). The resulting mixture was stirred at 90 °C for 2 h; after cooling to room temperature, 50 mL of water was added and extracted by CH_2Cl_2 (3 × 10 mL). Combined organic layers were dried over $MgSO_4$, filtered, and concentrated under a vacuum. The crude mixture was purified by silica gel chromatography (petroleum ether/AcOEt = 4/1) to give **7** as a white solid (49.3 mg, 15.1%). HPLC: 3.75 min, 99.3%; mp 152.2–153.7 °C. ^{1}H NMR (400 MHz, $CDCl_3$) δ 7.71 (d, J = 8.3 Hz, 2H), 7.17 (d, J = 8.2 Hz, 2H), 6.85–6.81 (m, 2H), 6.78–6.74 (m, 2H), 4.95 (s, 2H), 4.41 (s, 1H). ^{13}C NMR (101 MHz, $CDCl_3$) δ 152.75, 149.83, 137.65, 137.00, 129.27, 116.09, 115.91, 93.35, 70.11. MS (EI): m/z calcd for $C_{13}H_{11}IO_2$ 326; found 326 M^+ (different from the procedure in ref 45, 4-(4-iodobenzyloxy)phenol was gained though a SN2 reaction between hydroquinone and 1-(bromomethyl)-4-iodobenzene).

*3-(4-Iodobenzyloxy)phenol (**8**).* The procedure described above for the preparation of **7** was employed to afford **8** as a white solid (93.1 mg, 28.5%). HPLC: 3.95 min, 98.6%; mp 109.9–110.6 °C. ^{1}H NMR (400 MHz, $CDCl_3$) δ 7.71 (d, J = 7.9 Hz, 2H), 7.17 (d, J = 8.2 Hz, 2H), 7.16–7.09 (m, 1H), 6.54 (d, J = 8.6 Hz, 1H), 6.46–6.44 (m, 2H), 4.98 (s, 2H), 4.74 (s, 1H). ^{13}C NMR (101 MHz, $CDCl_3$) δ 159.87, 156.65, 137.67, 136.59, 130.24, 129.23, 108.32, 107.39, 102.55, 93.45, 69.36. MS (EI): m/z calcd for $C_{13}H_{11}IO_2$ 326; found 326 M^+.

*2-(4-Iodobenzyloxy)phenol (**9**).* The procedure described above for the preparation of **7** was employed to afford **9** as yellow oil (109.8 mg, 33.7%). HPLC: 4.25 min, 99.9%; mp 62.1–63.4 °C. ^{1}H NMR (400 MHz, $CDCl_3$) δ 7.74 (d, J = 8.2 Hz, 2H), 7.17 (d, J = 8.0 Hz, 2H), 6.98–6.95 (m, 1H), 6.93–6.88 (m, 2H), 6.85–6.81 (m, 1H), 5.62 (s, 1H), 5.06 (s, 2H). ^{13}C NMR (101 MHz, $CDCl_3$) δ 145.91, 145.56, 137.88, 136.09, 129.54, 122.13, 120.20, 114.98, 112.30, 93.99, 70.44. MS (EI): m/z calcd for $C_{13}H_{11}IO_2$ 326; found 326 M^+.

*1-Fluoro-4-(4-iodobenzyloxy)benzene (**10**).* The procedure described above for the preparation of **1** was employed to afford **10** as a white solid (253.1 mg, 77.1%). HPLC: 8.92 min, 98.0%; mp 62.3–62.8 °C. ^{1}H NMR (400 MHz, $CDCl_3$) δ 7.72 (d, J = 8.2 Hz, 2H), 7.17 (d, J = 8.2 Hz, 2H), 7.00–6.95 (m, 2H), 6.91–6.85 (m, 2H), 4.97 (s, 2H). ^{13}C NMR (101 MHz, $CDCl_3$) δ 157.49 (d, J = 238.9 Hz, 1C), 154.61 (d, J = 2.1 Hz, 1C), 137.71, 136.58, 129.23, 115.95 (d, J = 12.3 Hz, 2C), 115.88 (d, J = 18.8 Hz, 2C), 93.51, 70.00. MS (EI): m/z calcd for $C_{13}H_{10}FIO$ 328; found 328 M^+.

*1-Chloro-4-(4-iodobenzyloxy)benzene (**11**).* The procedure described above for the preparation of **1** was employed to afford **11** as a white solid (136.2 mg, 79.0%). HPLC: 12.86 min, 99.6%; mp 107.5–108.1 °C. ^{1}H NMR (400 MHz, $CDCl_3$) δ 7.72 (d, J = 8.2 Hz, 2H), 7.24 (d, J = 8.9 Hz, 2H), 7.16 (d, J = 8.2 Hz, 2H), 6.87 (d, J = 8.9 Hz, 2H), 4.98 (s, 2H). ^{13}C NMR (101 MHz, $CDCl_3$) δ 157.06, 137.72, 136.30, 129.40, 129.19, 126.08, 116.15, 93.59, 69.60. MS (EI): m/z calcd for $C_{13}H_{10}ClIO$ 344; found 344 M^+.

*1-Bromo-4-(4-iodobenzyloxy)benzene (**12**).* The procedure described above for the preparation of **1** was employed to afford **12** as a white solid (302.5 mg, 77.8%). HPLC: 14.61 min, 99.3%; mp 122.6–123.5 °C. ^{1}H NMR (400 MHz, $CDCl_3$) δ 7.71 (d, J = 8.2 Hz, 2H), 7.37 (d, J = 9.0 Hz, 2H), 7.16 (d, J = 8.2 Hz, 2H), 6.82 (d, J = 8.9 Hz, 2H), 4.97 (s, 2H). ^{13}C NMR (101 MHz, $CDCl_3$) δ 157.58, 137.74, 136.26, 132.35, 129.20, 116.68, 113.39, 93.62, 69.53. MS (EI): m/z calcd for $C_{13}H_{10}BrIO$ 388; found 388 M^+ (compared with the method in ref 46, the reaction was carried out in DMF instead of acetone and gave 1-bromo-4-(4-iodobenzyloxy)benzene in a higher yield of 77.8%).

*1-Iodo-4-(4-iodobenzyloxy)benzene (**13**).* The procedure described above for the preparation of **1** was employed to afford **13** as a white solid (436.0 mg, 89.3%). HPLC: 17.49 min, 98.2%; mp 135.0–135.9 °C. ^{1}H NMR (400 MHz, $CDCl_3$) δ 7.71 (d, J = 8.2 Hz, 2H), 7.56 (d, J = 8.7 Hz, 2H), 7.15 (d, J = 8.1 Hz, 2H), 6.72 (d, J = 8.8 Hz, 2H), 4.97 (s, 2H). ^{13}C NMR (101 MHz, $CDCl_3$) δ 158.33, 138.29, 137.72, 136.21, 129.17, 117.25, 93.60, 83.31, 69.37. MS (EI): m/z calcd for $C_{13}H_{10}I_2O$ 436; found 436 M^+.

*1-Iodo-4-(phenoxymethyl)benzene (**14**).* The procedure described above for the preparation of **1** was employed to afford **14** as a white solid (310.1 mg, 72.1%). HPLC: 9.59 min, 99.2%; mp 96.7–97.6 °C. ^{1}H NMR (400 MHz, $CDCl_3$) δ 7.72 (d, J = 8.2 Hz, 2H), 7.32–7.27 (m, 2H), 7.19 (d, J = 8.1 Hz, 2H), 6.99–6.94 (m, 3H), 5.02 (s, 2H). ^{13}C NMR (101 MHz, $CDCl_3$) δ 158.49, 137.64, 136.81, 129.51, 129.22, 121.15, 114.84, 93.37, 69.20. MS (EI): m/z calcd for $C_{13}H_{11}IO$ 310; found 310 M^+ (different from the procedure in ref 47, 1-iodo-4-(phenoxymethyl)benzene was gained though a SN2 reaction between phenol and 1-(bromomethyl)-4-iodobenzene).

*1-tert-Butyl-4-(4-iodobenzyloxy)benzene (**15**).* The procedure described above for the preparation of **1** was employed to afford **15** as a white solid (366.2 mg, 87.4%). HPLC: 27.14 min, 98.3%; mp 91.9–93.0 °C. ^{1}H NMR (400 MHz, $CDCl_3$) δ 7.71 (d, J = 8.2 Hz, 2H), 7.31 (d, J = 8.8 Hz, 2H), 7.18 (d, J = 8.2 Hz, 2H), 6.89 (d, J = 8.8 Hz, 2H), 4.99 (s, 2H), 1.30 (s, 9H). ^{13}C NMR (101 MHz, $CDCl_3$) δ 156.28,

dx.doi.org/10.1021/jm5004396 | J. Med. Chem. XXXX, XXX, XXX–XXX

143.85, 137.62, 137.04, 129.23, 126.28, 114.26, 93.29, 69.30, 34.07, 31.50. MS (EI): m/z calcd for $C_{17}H_{19}IO$ 366; found 366 M^+.

*4-(4-Iodobenzyloxy)aniline (**16**).* To a solution of **1** (1.42 g, 4.0 mmol) and $SnCl_2{\cdot}2H_2O$ (1.66 g, 8.0 mmol) in EtOH (25 mL) was added concentrated HCl (2 mL). The resulting mixture was stirred at 80 °C for 2 h; after cooling to room temperature, 1 M NaOH (30 mL) was added and extracted by ethyl acetate (3 × 10 mL). Combined organic layers were dried over $MgSO_4$, filtered, and concentrated under a vacuum. The crude mixture was purified by silica gel chromatography (petroleum ether/AcOEt = 2/1) to give **16** as a pink solid (643.3 mg, 49.5%). HPLC: 4.16 min, 98.4%; mp 138.6−140.0 °C. ^{1}H NMR (400 MHz, $CDCl_3$) δ 7.70 (d, J = 8.2 Hz, 2H), 7.16 (d, J = 7.9 Hz, 2H), 6.78 (d, J = 8.7 Hz, 2H), 6.64 (d, J = 8.8 Hz, 2H), 4.93 (s, 2H), 3.44 (s, 2H). ^{13}C NMR (101 MHz, DMSO-d_6) δ 149.39, 142.65, 137.65, 137.02, 129.66, 115.75, 114.84, 93.42, 69.11. MS (EI): m/z calcd for $C_{13}H_{12}INO$ 325; found 325 M^+.

*3-(4-Iodobenzyloxy)aniline (**17**).* The procedure described above for the preparation of **16** was employed to afford **17** as a white solid (695.5 mg, 73.1%). HPLC: 4.50 min, 99.4%; mp 153.9−154.8 °C. ^{1}H NMR (400 MHz, $CDCl_3$) δ 7.70 (d, J = 8.1 Hz, 2H), 7.17 (d, J = 8.0 Hz, 2H), 7.07 (t, J = 8.0 Hz, 1H), 6.40−6.34 (m, 3H), 4.97 (s, 2H). ^{13}C NMR (101 MHz, DMSO-d_6) δ 158.95, 143.26, 137.13, 136.95, 129.97, 129.69, 110.51, 106.88, 104.24, 93.73, 68.31. MS (EI): m/z calcd for $C_{13}H_{12}INO$ 325; found 325 M^+.

*2-(4-Iodobenzyloxy)aniline (**18**).* The procedure described above for the preparation of **16** was employed to afford **18** as a white solid (99.3 mg, 11.4%). HPLC: 4.88 min, 99.1%; mp 99.1−100.1 °C. ^{1}H NMR (400 MHz, $CDCl_3$) δ 7.71 (d, J = 8.3 Hz, 2H), 7.19 (d, J = 8.3 Hz, 2H), 6.85−6.78 (m, 3H), 6.75−6.71 (m, 1H), 5.03 (s, 2H). ^{13}C NMR (101 MHz, $CDCl_3$) δ 146.14, 137.66, 136.90, 136.48, 129.34, 121.73, 118.39, 115.30, 112.14, 93.46, 69.73. MS (EI): m/z calcd for $C_{13}H_{12}INO$ 325; found 325 M^+.

*4-(4-Iodobenzyloxy)-N-methylaniline (**19**).* A solution of $NaOCH_3$ (54.0 mg, 1.0 mmol) in methanol (5 mL) was added to a mixture of **16** (162.6 mg, 0.5 mmol) and paraformaldehyde (60.0 mg, 2.0 mmol) in methanol (30 mL) dropwise. The resulting mixture was stirred under reflux for 2 h. After cooling to room temperature, $NaBH_4$ (75.6 mg, 2.0 mmol) was added and the solution was stirred under reflux for 2 h. The solvent was evaporated under a vacuum. Then 1 M NaOH (50 mL) was added and a white precipitate was formed. The precipitate was collected by filtration, washed with 50 mL water, and recrystallized from methanol to give **19** as a pink solid (152.4 mg, 89.9%). HPLC: 6.34 min, 99.2%; mp 93.9−95.2 °C. ^{1}H NMR (400 MHz, $CDCl_3$) δ 7.70 (d, J = 8.2 Hz, 2H), 7.17 (d, J = 8.1 Hz, 2H), 6.84 (d, J = 8.7 Hz, 2H), 6.58 (d, J = 8.5 Hz, 2H), 4.94 (s, 2H), 2.81 (s, 3H). ^{13}C NMR (101 MHz, $CDCl_3$) δ 150.89, 144.11, 137.55, 137.42, 129.28, 116.23, 116.21, 113.50, 93.16, 70.26, 70.24, 31.49. MS (EI): m/z calcd for $C_{14}H_{14}INO$ 339; found 339 M^+.

*3-(4-Iodobenzyloxy)-N-methylaniline (**20**).* A solution of $NaOCH_3$ (54.0 mg, 1.0 mL) in methanol (5 mL) was added to a mixture of **17** (162.6 mg, 0.5 mmol) and paraformaldehyde (60.0 mg, 2.0 mmol) in methanol (30 mL) dropwise. The resulting mixture was stirred under reflux for 2 h. After cooling to room temperature, $NaBH_4$ (75.6 mg, 2.0 mmol) was added and the solution was stirred under reflux for 2 h. The solvent was evaporated under a vacuum. Then 1 M NaOH (50 mL) was added and extracted by CH_2Cl_2 (3 × 10 mL). Combined organic layers were dried over $MgSO_4$, filtered, and concentrated under a vacuum. The crude mixture was purified by silica gel chromatography (petroleum ether/AcOEt = 4/1) to give **20** as a colorless oil (71.0 mg, 41.8%). HPLC: 6.60 min, 99.9%; mp 45.3−46.6 °C. ^{1}H NMR (400 MHz, $CDCl_3$) δ 7.71 (d, J = 8.1 Hz, 2H), 7.19 (d, J = 8.0 Hz, 2H), 7.09 (t, J = 8.0 Hz, 1H), 6.32 (d, J = 8.0 Hz, 1H), 6.27 (d, J = 7.9 Hz, 1H), 6.24 (s, 1H), 4.99 (s, 2H), 2.83 (s, 3H). ^{13}C NMR (101 MHz, $CDCl_3$) δ 159.84, 150.77, 137.59, 137.09, 129.94, 129.25, 106.16, 103.06, 99.24, 93.26, 69.11, 30.68. MS (EI): m/z calcd for $C_{14}H_{14}INO$ 339; found 339 M^+.

*2-(4-Iodobenzyloxy)-N-methylaniline (**21**).* To a solution of **18** (50.0 mg, 0.15 mmol) and K_2CO_3 (41.5 mg, 0.30 mmol) in acetone (10 mL) was added CH_3I (32.6 mg, 0.23). The resulting mixture was stirred at room temperature for 10 h. Then 50 mL water was added and extracted by CH_2Cl_2 (3 × 10 mL). Combined organic layers were dried over $MgSO_4$, filtered, and concentrated under a vacuum. The crude mixture was purified by silica gel chromatography (petroleum ether/AcOEt = 4/1) to give **21** as a yellow oil (34.2 mg, 67.2%). HPLC: 8.19 min, 98.1%. ^{1}H NMR (400 MHz, $CDCl_3$) δ 7.71 (d, J = 8.3 Hz, 2H), 7.17 (d, J = 8.4 Hz, 2H), 6.92 (td, J = 7.7, 1.3 Hz, 1H), 6.78 (d, J = 7.9 Hz, 1H), 6.66−6.60 (m, 2H), 5.00 (s, 2H), 4.24 (s, 1H), 2.85 (s, 3H). ^{13}C NMR (101 MHz, $CDCl_3$) δ 145.77, 139.59, 137.66, 136.88, 129.43, 121.96, 116.15, 110.88, 109.60, 93.48, 69.72, 30.31. MS (EI): m/z calcd for $C_{14}H_{14}INO$ 339; found 339 M^+.

*4-(4-Iodobenzyloxy)-N,N-dimethylaniline (**22**).* To a solution of **16** (162.6 mg, 0.5 mmol) and paraformaldehyde (150.0 mg, 5.0 mmol) in acetic acid (20 mL) was added $NaBH_3CN$ (157.0 mg, 2.5). The resulting mixture was stirred at room temperature for 24 h. Then 1 M NaOH (20 mL) was added and a white precipitate was formed. The precipitate was collected by filtration, washed with 50 mL water, and recrystallized from methanol to give **22** as a white solid (168.4 mg, 95.4%). HPLC: 10.63 min, 98.4%; mp 128.2−129.3 °C. ^{1}H NMR (400 MHz, $CDCl_3$) δ 7.69 (d, J = 8.2 Hz, 2H), 7.17 (d, J = 8.0 Hz, 2H), 6.88 (d, J = 8.9 Hz, 2H), 6.82−6.68 (s, 2H), 4.95 (s, 2H), 2.87 (s, 6H). ^{13}C NMR (101 MHz, $CDCl_3$) δ 150.92, 145.99, 137.59, 137.41, 129.28, 115.95, 114.77, 93.19, 70.16, 41.73. HRMS (EI): m/z calcd for $C_{15}H_{16}INO$ 353.0277; found 353.0282 M^+.

*3-(4-Iodobenzyloxy)-N,N-dimethylaniline (**23**).* The procedure described above for the preparation of **22** was employed to afford **23** as a white solid (171.3 mg, 97.1%). HPLC: 11.30 min, 99.9%; mp 68.8−70.1 °C. ^{1}H NMR (400 MHz, $CDCl_3$) δ 7.71 (d, J = 8.2 Hz, 2H), 7.19 (d, J = 8.2 Hz, 2H), 7.15 (t, J = 8.1 Hz, 1H), 6.43−6.30 (m, 3H), 5.00 (s, 2H), 2.94 (s, 6H). ^{13}C NMR (101 MHz, $CDCl_3$) δ 159.68, 152.02, 137.62, 137.18, 129.77, 129.31, 106.15, 102.16, 100.03, 93.26, 69.20, 40.55. MS (EI): m/z calcd for $C_{15}H_{16}INO$ 353; found 353 M^+.

*1-Iodo-4-(4-methoxybenzyloxy)benzene (**24**).* The procedure described above for the preparation of **1** was employed to afford **24** as a white solid (906.3 mg, 88.9%). HPLC: 8.55 min, 99.7%; mp 130.3−131.5 °C. ^{1}H NMR (400 MHz, $CDCl_3$) δ 7.55 (d, J = 9.0 Hz, 2H), 7.33 (d, J = 8.7 Hz, 2H), 6.91 (d, J = 8.7 Hz, 2H), 6.74 (d, J = 8.9 Hz, 2H), 4.95 (s, 2H), 3.81 (s, 3H). ^{13}C NMR (101 MHz, $CDCl_3$) δ 159.59, 158.71, 138.22, 129.19, 128.55, 117.36, 114.08, 82.95, 69.91, 55.31. HRMS (EI): m/z calcd for $C_{14}H_{13}IO_2$ 339.9960; found 339.9964 M^+ (compared with the method in ref 48, the reaction was carried out in DMF without the use of tetra-*n*-butylammonium iodide and gave 1-iodo-4-(4-methoxybenzyloxy)benzene in a comparable yield).

*(4-Iodobenzyl)(4-methoxyphenyl)sulfane (**25**).* The procedure described above for the preparation of **1** was employed to afford **25** as a white solid (712.4 mg, 94.7%); mp 87.9−88.5 °C. ^{1}H NMR (400 MHz, $CDCl_3$) δ 7.56 (d, J = 8.3 Hz, 2H), 7.23 (d, J = 8.8 Hz, 2H), 6.90 (d, J = 8.3 Hz, 2H), 6.79 (d, J = 8.8 Hz, 2H), 3.89 (s, 2H), 3.78 (s, 3H). ^{13}C NMR (101 MHz, $CDCl_3$) δ 159.40, 137.99, 137.39, 134.38, 130.81, 125.39, 114.51, 92.32, 55.30, 40.76. MS (EI): m/z calcd for $C_{14}H_{13}IOS$ 356; found 356 M^+.

*1-Bromo-4-((4-methoxyphenoxy)methyl)benzene (**26**).* The procedure described above for the preparation of **1** was employed to afford **26** as a white solid (2.93 g, 93.2%); mp 105.3−106.7 °C. ^{1}H NMR (400 MHz, $CDCl_3$) δ 7.51 (d, J = 8.3 Hz, 2H), 7.30 (d, J = 8.3 Hz, 2H), 6.89 (d, J = 9.2 Hz, 2H), 6.83 (d, J = 9.2 Hz, 2H), 4.97 (s, 2H), 3.77 (s, 3H). ^{13}C NMR (101 MHz, $CDCl_3$) δ 154.15, 152.65, 136.38, 131.65, 129.05, 121.74, 115.89, 114.70, 69.97, 55.70. MS (EI): m/z calcd for $C_{14}H_{13}BrO_2$ 292; found 292 M^+.

*1-Bromo-4-(4-methoxybenzyloxy)benzene (**27**).* The procedure described above for the preparation of **1** was employed to afford **27** as a white solid (681.4 mg, 77.8%); mp 122.1−122.9 °C. ^{1}H NMR (400 MHz, $CDCl_3$) δ 7.37 (d, J = 9.0 Hz, 2H), 7.33 (d, J = 8.7 Hz, 2H), 6.91 (d, J = 8.7 Hz, 2H), 6.84 (d, J = 9.0 Hz, 2H), 4.96 (s, 2H), 3.82 (s, 3H). ^{13}C NMR (101 MHz, $CDCl_3$) δ 159.57, 157.93, 132.25, 129.19, 128.57, 116.74, 114.06, 113.03, 70.04, 55.30. MS (EI): m/z calcd for $C_{14}H_{13}BrO_2$ 292; found 292 M^+ (compared with the method in ref 49, 1-bromo-4-(4-methoxybenzyloxy)benzene was prepared though a common SN2 reaction between 4-bromophenol and 1-(chloromethyl)-4-methoxybenzene in a comparable yield).

*4-(4-Bromobenzyloxy)-N,N-dimethylaniline (**28**).* The procedure described above for the preparation of **1** was employed to afford **28** as a

dx.doi.org/10.1021/jm5004396 | J. Med. Chem. XXXX, XXX, XXX−XXX

white solid (303.5 mg, 99.1%); mp 125.8−127.1 °C. ^{1}H NMR (400 MHz, $CDCl_3$) δ 7.52−7.48 (m, 2H), 7.32−7.28 (m, 2H), 6.92−6.85 (m, 2H), 6.76 (s, 2H), 4.96 (s, 2H), 2.88 (s, 6H). ^{13}C NMR (101 MHz, DMSO-d_6) δ 149.92, 145.65, 137.14, 131.20, 129.56, 120.60, 115.62, 114.09, 68.84, 41.00. MS (EI): m/z calcd for $C_{15}H_{16}BrNO$ 305; found 305 M^+.

*Tributyl(4-((4-methoxyphenoxy)methyl)phenyl)stannane (**29**).* A mixture of **25** (146.6 mg, 0.5 mmol), $(Bu_3Sn)_2$ (580.1 mg, 1.0 mmol), and $(Ph_3P)_4Pd$ (57.8 mg, 0.05 mmol) in toluene (10 mL) was stirred under reflux overnight. The mixture was concentrated under a vacuum and purified by silica gel chromatography (petroleum ether/AcOEt = 15/1) to give **29** as a colorless oil (89.5 mg, 35.6%). ^{1}H NMR (400 MHz, $CDCl_3$) δ 7.49 (d, J = 7.9 Hz, 2H), 7.39 (d, J = 7.8 Hz, 2H), 6.93 (d, J = 9.1 Hz, 2H), 6.85 (d, J = 9.1 Hz, 2H), 5.00 (s, 2H), 3.78 (s, 3H), 1.59−1.51 (m, 6H), 1.39−1.29 (m, 6H), 1.15−0.97 (m, 6H), 0.90 (t, J = 7.3 Hz, 9H). ^{13}C NMR (101 MHz, $CDCl_3$) δ 153.96, 153.11, 141.68, 136.90, 136.67, 127.08, 115.83, 114.65, 70.83, 55.72, 29.09, 27.38, 13.67, 9.60. MS (EI): m/z calcd for $C_{26}H_{40}O_2Sn$ 504; found 504 M^+.

*Tributyl(4-(4-methoxybenzyloxy)phenyl)stannane (**30**).* The procedure described above for the preparation of **29** was employed to afford **30** as a colorless oil (75.0 mg, 29.8%). ^{1}H NMR (400 MHz, $CDCl_3$) δ 7.40−7.32 (m, 3H), 7.31−7.27 (m, 1H), 6.99−6.95 (m, 2H), 6.91 (d, J = 8.4 Hz, 2H), 4.98 (s, 2H), 3.82 (s, 3H), 1.69−1.60 (m, 6H), 1.41−1.30 (m, 12H), 0.92 (t, J = 7.3 Hz, 9H); ^{13}C NMR (101 MHz, $CDCl_3$) δ 153.98, 153.12, 141.68, 136.91, 136.66, 127.07, 115.85, 114.67, 70.85, 55.73, 29.09, 27.38, 13.66, 9.60. MS (EI): m/z calcd for $C_{26}H_{40}O_2Sn$ 504; found 504 M^+.

*N,N-Dimethyl-4-((4-(tributylstannyl)benzyl)oxy)aniline (**31**).* The procedure described above for the preparation of **29** was employed to afford **31** as a colorless oil (56.2 mg, 21.8%). ^{1}H NMR (400 MHz, $CDCl_3$) δ 7.47 (d, J = 7.9 Hz, 2H), 7.38 (d, J = 7.9 Hz, 2H), 6.92 (d, J = 9.1 Hz, 2H), 6.74 (d, J = 8.9 Hz, 2H), 4.98 (s, 2H), 2.87 (s, 6H), 1.58−1.50 (m, 6H), 1.38−1.28 (m, 6H), 1.11−0.97 (m, 6H), 0.88 (t, J = 7.3 Hz, 9H) ^{13}C NMR (101 MHz, $CDCl_3$) δ 151.32, 145.96, 141.49, 137.24, 136.63, 127.10, 115.84, 114.76, 70.90, 41.74, 29.09, 27.38, 13.66, 9.60. MS (EI): m/z calcd for $C_{27}H_{43}NOSn$ 517; found 517 M^+.

X-ray Crystallography. 50 mg of ligand **4** and **6** were dissolved in 3 mL of ethyl acetate, respectively. Upon slow evaporation at room temperature, colorless crystals suitable for an X-ray diffraction analysis were yielded. The X-ray single-crystal structures were determined on a Bruker Smart APEXII CCD area-detector diffractometer at 100(2) or 150(2) K with graphite monochromated Mo Kα radiation (λ = 0.71073 Å). Absorption correction was performed by the SADABS program.[27] All structures were solved using SHELXL-97[28] program and refined with full-matrix least-squares on F^2 method. All the hydrogen atoms were geometrically fixed using the riding model.

Radiolabeling and Bioevaluation. The radio-iodinated ligands **4**, **24**, and **22** were prepared from the corresponding tributyltin derivatives by iododestannylation reaction through previously reported method.[29]

Bioevaluation including binding assay in vitro using Aβ aggregates, autoradiography in vitro using brain sections from AD patients and transgenic model mice, biodistribution studies, and partition coefficient determination were all conducted according to previously reported methods.[30]

K_d determination for [^{125}I]**4**: Peptides Aβ_{42} were purchased from Osaka Peptide Institute (Osaka, Japan). Aggregation was performed according to the procedure described previously.[30] Saturation binding assay was set up by adding 100 μL of Aβ_{42} aggregates (10 nM in the final assay mixture) into a mixture containing 100 μL of different concentrations of [^{125}I]**4** (final concentrations vary from 0.2 to 1.2 nM), 100 μL of EtOH, and a corresponding amount of 0.1% bovine serum albumin in a final volume of 1 mL. While for nonspecific binding group, an additional 100 μL of cold **4** was added in a final concentration of 1 μM. After incubation for 3 h at room temperature, the bound and free radioactive fractions were separated by vacuum filtration through glass fiber filters (Whatman GF/B) using a Mp-48T cell harvester (Brandel, Gaithersburg, MD). The radioactivity of filters containing the bound ^{125}I-ligand was measured in an automatic γ-counter (WALLAC/Wizard1470, USA) with 70% efficiency. The dissociation constant K_d for [^{125}I]**4** was determined by analysis of the saturation binding curves of three independent assays with GraphPad Prism 5.0.

In vitro biostability in mouse plasma and liver homogenate: [^{125}I]**4** (30 μCi, in 30 μL of ethanol) was added to 300 μL of mouse plasma and liver homogenate separately and then incubated at 37 °C for 2, 10, 30, and 60 min. After that, 300 μL of acetonitrile was added to each sample followed by filtration using nylon syringe filters (13 mm × 0.22 μm, Troody, China) to remove the denatured proteins. The filtrates were analyzed by HPLC. Biostability of [^{125}I]IMPY in plasma was conducted in the same way.

In vivo biostability of [^{125}I]**4**: Four ICR mice were injected [^{125}I]**4** (250 μCi, 200 μL) via tail vein and sacrificed at 2, 10, 30, and 60 min postinjection. Then 2 mL blood sample was collected and centrifuged at 3000 rpm for 3 min to separate plasma. Urine was also harvested. Brain, liver, and feces were obtained and homogenized in physiological saline. Subsequently, 200 μL of each sample was removed and mixed with 300 μL of acetonitrile, and then samples were analyzed with the identify method as described for in vitro biostability.

Computational Methods. Ligands **4** and **6** with X-ray crystal structural data were directly minimized to the nearest ground states using hybrid density functional technique B3LYP[31,32] with basis set 3-21G[33] for iodine and 6-31G[34] for other atoms in Gaussian 09[35] with tight convergence. The RMSD values between the optimized structures and the geometries of corresponding X-ray crystallographic structures were calculated using VMD 1.9.1 software[36] after alignment. The remaining 19 molecules were constructed with GaussView 5.0 and geometry optimized with the same method.

CoMFA and CoMSIA analysis was carried out to generate good predictive QSAR models using SYBYL-X 1.1 software[37] according to method reported previously with some modifications.[38] Gasteiger−Hückel charges were assigned to all the QM-optimized molecules. Structural alignment was performed by using most promising compound **4** as a template and benzyloxybenzene backbone (Figure 2a) as a common structure. The aligned molecules are shown in Figure 2b. The pK_i values of 21 benzyloxybenzene ligands in Table 1, which covered a range of 3 log units, were used as dependent variables. These pK_i values were imported into a molecular spreadsheet, and then the Tripos standard CoMFA/CoMSIA fields were added to the spreadsheet. Compared with CoMFA, three additional descriptors (hydrophobic and hydrogen-bond donor and acceptor) were also defined in CoMSIA method. Default parameters were used for constructing 3D-QSAR models. Partial least-squares (PLS) methods were utilized to construct 3D-QSAR models. The PLS algorithmic rule with leave-one-out cross-validation method was applied to gain optimum number of components, cross-validated coefficient q^2 and to evaluate the statistical significance of each model. Column filter value was set to 1.0 kcal/mol for all cross-validated PLS analyses. Conventional correlation coefficient (r^2), and its standard error (SEE), F-test value (F) were further computed by PLS analysis with no validation method.

AutoDock4.0[39−41] was employed to conduct the docking simulations on a solid-state NMR-derived model of an Aβ fiber (PDB 2LMO).[42] All hydrogen atoms were added and Gasteiger charges[43] were assigned to the receptor using AutoDock Tools (ADT).[44] QM-optimized IMPY and several benzyloxybenzene analogues with various binding affinities were served as the input ligands. Nonpolar hydrogen atoms were merged and all torsions were set to be rotatable during docking. Residues 16-KLVFFA-21 of the Aβ_{40} fiber were chosen for docking, and each grid was centered on this site. Grid maps were generated using AutoGrid 4.0 with 34 × 62 × 80 Å^3 dimensions and a grid spacing of 0.375 Å, which was large enough to encompass the entire chosen site.[39] Lamarckian genetic algorithm was applied for searching the lowest energy binding conformations with the default parameters from AutoDock4.0.[39] The binding energy is a value representing the fitness of the ligand with the protein, which integrates a set of state variables including values describing the translation, orientation, and conformation of the ligand. It is evaluated using the energy function. Then 100 GA ran with a population size of 300, a maximum of 2.5 × 10^7 energy evaluations, and a maximum of 27000 generations. The resulting 100 solutions from docking were clustered into groups with RMS deviations lower than 1.0 Å, and the lowest-energy/top-ranked docked pose was

dx.doi.org/10.1021/jm5004396 | J. Med. Chem. XXXX, XXX, XXX−XXX

extracted as the best conformation for each ligand. We confirmed that the best conformation for each ligand was located in the identical position of Aβ_{40} fiber with similar orientation.

■ ASSOCIATED CONTENT

Supporting Information

Additional tables, figures, NMR/MS spectra, and CIF files. This material is available free of charge via the Internet at http://pubs.acs.org.

■ AUTHOR INFORMATION

Corresponding Author

*Phone/Fax: +86-10-58808891. E-mail: cmc@bnu.edu.cn.

Author Contributions

Conceived and designed the experiments: M. Cui and B. Liu. Performed the experiments: Y. Yang, M. Cui and X. Zhang. Analyzed the data: Y. Yang, X. Zhang. Contributed reagents/materials/analysis tools: M. Cui, B. Liu, J. Dai, Z. Zhang, C. Lin and Y. Guo. Wrote the paper: Y. Yang, M. Cui and B. Liu.

Notes

The authors declare no competing financial interest.

■ ACKNOWLEDGMENTS

This work was funded by the National Natural Science Foundation of China (no. 21201019) and the Fundamental Research Funds for the Central Universities (no. 2012LYB19). We thank Dr. Jin Liu (College of Life Science, Beijing Normal University) for assistance in the in vitro neuropathologueical staining, and Prof. Huabei Zhang, Prof. Yan Wang, and Dr. Shiyuan Hu (College of Chemistry, Beijing Normal University) for assistance in the computional experiments.

■ ABBREVIATIONS USED

AD, Alzheimer's disease; Aβ, β-amyloid; PET, positron emission tomography; SPECT, single photon emission computed tomography; CR, Congo red; ThT, thioflavin T; BBB, blood−brain barrier; PIB, 2-(4-(methylamino)phenyl)benzo[*d*]thiazol-6-ol; U.S. FDA, United States Food and Drug Administration; IMPY, 4-(6-iodoimidazo[1,2-*a*]pyridin-2-yl)-*N*,*N*-dimethylaniline; B3LYP, 3-parameter hybrid Becke exchange/Lee−Yang−Parr correlation functional; RMSD, root-mean-square deviations; 3D-QSAR, three-dimensional quantitative structure−activity relationship; CoMFA, comparative molecular field analysis; CoMSIA, comparative molecular similarity indices analysis; NMR, nuclear magnetic resonance; *J*, coupling constant (in NMR spectrometry); MS (EI), mass spectrometry (electron ionization); HRMS, high-resolution mass spectrometry; HPLC, high-performance liquid chromatography; DMF, *N*,*N*-dimethylformamide; QM, quantum mechanics; PLS, partial least-squares; ADT, autodock tools; GA, genetic algorithm

■ REFERENCES

(1) Brookmeyer, R.; Johnson, E.; Ziegler-Graham, K.; Arrighi, H. M. Forecasting the global burden of Alzheimer's disease. *Alzheimer's Dementia* **2007**, *3*, 186−191.

(2) Hardy, J.; Selkoe, D. J. The amyloid hypothesis of Alzheimer's disease: progress and problems on the road to therapeutics. *Science* **2002**, *297*, 353−356.

(3) Han, H.; Cho, C.-G.; Lansbury, P. T. Technetium complexes for the quantitation of brain amyloid. *J. Am. Chem. Soc.* **1996**, *118*, 4506−4507.

(4) Raimon, S.; Joan, E. Pinacyanol as effective probe of fibrillar beta-amyloid peptide: comparative study with Congo Red. *Biopolymers* **2003**, *72*, 455−463.

(5) Kadir, A.; Marutle, A.; Gonzalez, D.; Schöll, M.; Almkvist, O.; Mousavi, M.; Mustafiz, T.; Darreh-Shori, T.; Nennesmo, I.; Nordberg, A. Positron emission tomography imaging and clinical progression in relation to molecular pathologuey in the first Pittsburgh Compound B positron emission tomography patient with Alzheimer's disease. *Brain* **2011**, *134*, 301−317.

(6) Koole, M.; Lewis, D. M.; Buckley, C.; Nelissen, N.; Vandenbulcke, M.; Brooks, D. J.; Vandenberghe, R.; Van Laere, K. Whole-body biodistribution and radiation dosimetry of ^{18}F-GE067: a radioligand for in vivo brain amyloid imaging. *J. Nucl. Med.* **2009**, *50*, 818−822.

(7) Okamura, N.; Shiga, Y.; Furumoto, S.; Tashiro, M.; Tsuboi, Y.; Furukawa, K.; Yanai, K.; Iwata, R.; Arai, H.; Kudo, Y.; Itoyama, Y.; Dohura, K. In vivo detection of prion amyloid plaques using [^{11}C]BF-227 PET. *Eur. J. Nucl. Med. Mol. Imaging* **2010**, *37*, 934−941.

(8) Chang, Y. S.; Jeong, J. M.; Lee, Y.-S.; Kim, H. W.; Ganesha, R. B.; Kim, Y. J.; Lee, D. S.; Chung, J.-K.; Lee, M. C. Synthesis and evaluation of benzothiophene derivatives as ligands for imaging β-amyloid plaques in Alzheimer's disease. *Nucl. Med. Biol.* **2006**, *33*, 811−820.

(9) Juréus, A.; Swahn, B.-M.; Sandell, J.; Jeppsson, F.; Johnson, A. E.; Johnström, P.; Neelissen, J. A. M.; Sunnemark, D.; Farde, L.; Svensson, S. P. S. Characterization of AZD4694, a novel fluorinated Aβ plaque neuroimaging PET radioligand. *J. Neurochem.* **2010**, *114*, 784−794.

(10) Kung, M.-P.; Hou, C.; Zhuang, Z.-P.; Zhang, B.; Skovronsky, D.; Trojanowski, J. Q.; Lee, V. M. Y.; Kung, H. F. IMPY: an improved thioflavin-T derivative for in vivo labeling of β-amyloid plaques. *Brain Res.* **2002**, *956*, 202−210.

(11) Cui, M.; Ono, M.; Kimura, H.; Kawashima, H.; Liu, B. L.; Saji, H. Radioiodinated benzimidazole derivatives as single photon emission computed tomography probes for imaging of β-amyloid plaques in Alzheimer's disease. *Nucl. Med. Biol.* **2011**, *38*, 313−320.

(12) Ono, M.; Wilson, A.; Nobrega, J.; Westaway, D.; Verhoeff, P.; Zhuang, Z.-P.; Kung, M.-P.; Kung, H. F. ^{11}C-labeled stilbene derivatives as Aβ-aggregate-specific PET imaging agents for Alzheimer's disease. *Nucl. Med. Biol.* **2003**, *30*, 565−571.

(13) Choi, S.; Golding, G.; Zhuang, Z.; Zhang, W.; Lim, N.; Hefti, F.; Benedum, T.; Kilbourn, M.; Skovronsky, D.; Kung, H. Preclinical properties of ^{18}F-AV-45: a PET agent for abeta plaques in the brain. *J. Nucl. Med.* **2009**, *50*, 1887−1894.

(14) Zhuang, Z.-P.; Kung, M.-P.; Hou, C.; Ploessl, K.; Kung, H. F. Biphenyls labeled with technetium 99m for imaging β-amyloid plaques in the brain. *Nucl. Med. Biol.* **2005**, *32*, 171−184.

(15) Wey, S.-P.; Weng, C.-C.; Lin, K.-J.; Yao, C.-H.; Yen, T.-C.; Kung, H. F.; Skovronsky, D.; Kung, M.-P. Validation of an ^{18}F-labeled biphenylalkyne as a positron emission tomography imaging agent for β-amyloid plaques. *Nucl. Med. Biol.* **2009**, *36*, 411−417.

(16) Watanabe, H.; Ono, M.; Ikeoka, R.; Haratake, M.; Saji, H.; Nakayama, M. Synthesis and biologueical evaluation of radioiodinated 2,5-diphenyl-1,3,4-oxadiazoles for detecting β-amyloid plaques in the brain. *Bioorg. Med. Chem.* **2009**, *17*, 6402−6406.

(17) Ryu, E. K.; Choe, Y. S.; Lee, K.-H.; Choi, Y.; Kim, B.-T. Curcumin and dehydrozingerone derivatives: synthesis, radiolabeling, and evaluation for β-amyloid plaque imaging. *J. Med. Chem.* **2006**, *49*, 6111−6119.

(18) Ono, M.; Yoshida, N.; Ishibashi, K.; Haratake, M.; Arano, Y.; Mori, H.; Nakayama, M. Radioiodinated flavones for in vivo imaging of β-amyloid plaques in the brain. *J. Med. Chem.* **2005**, *48*, 7253−7260.

(19) Ono, M.; Watanabe, R.; Kawashima, H.; Cheng, Y.; Kimura, H.; Watanabe, H.; Haratake, M.; Saji, H.; Nakayama, M. Fluoro-pegylated chalcones as positron emission tomography probes for in vivo imaging of β-amyloid plaques in Alzheimer's disease. *J. Med. Chem.* **2009**, *52*, 6394−6401.

(20) Ono, M.; Maya, Y.; Haratake, M.; Ito, K.; Mori, H.; Nakayama, M. Aurones serve as probes of β-amyloid plaques in Alzheimer's disease. *Biochem. Biophys. Res. Commun.* **2007**, *361*, 116−121.

(21) Camus, V.; Payoux, P.; Barré, L.; Desgranges, B.; Voisin, T.; Tauber, C.; Joie, R.; Tafani, M.; Hommet, C.; Chételat, G.; Mondon, K.;

Sayette, V.; Cottier, J. P.; Beaufils, E.; Ribeiro, M. J.; Gissot, V.; Vierron, E.; Vercouillie, J.; Vellas, B.; Eustache, F.; Guilloteau, D. Using PET with ^{18}F-AV-45 (florbetapir) to quantify brain amyloid load in a clinical environment. *Eur. J. Nucl. Med. Mol. Imaging* **2012**, *39*, 621−631.
(22) Barthel, H.; Gertz, H.; Dresel, S.; Peters, O.; Bartenstein, P.; Buerger, K.; Hiemeyer, F.; Wittemer-Rump, S.; Seibyl, J.; Reininger, C.; Sabri, O. Cerebral amyloid-beta PET with florbetaben (^{18}F) in patients with Alzheimer's disease and healthy controls: a multicentre phase 2 diagnostic study. *Lancet Neurol.* **2011**, *10*, 424−435.
(23) Newberg, A. B.; Wintering, N. A.; Plössl, K.; Hochold, J.; Stabin, M. G.; Watson, M.; Skovronsky, D.; Clark, C. M.; Kung, M.-P.; Kung, H. F. Safety, biodistribution, and dosimetry of ^{123}I-IMPY: a novel amyloid plaque−imaging agent for the diagnosis of Alzheimer's disease. *J. Nucl. Med.* **2006**, *47*, 748−754.
(24) Eckroat, T. J.; Mayhoub, A. S.; Garneau-Tsodikova, S. Amyloid-β probes: review of structure−activity and brain-kinetics relationships. *Beilstein J. Org. Chem.* **2013**, *9*, 1012−1044.
(25) Cui, M. Past and recent progress of molecularimaging probes for β-amyloid plaques in the brain. *Curr. Med. Chem.* **2014**, *21*, 82−112.
(26) Cook, N. P.; Ozbil, M.; Katsampes, C.; Prabhakar, R.; Martí, A. A. Unraveling the photoluminescence response of light-switching ruthenium(II) complexes bound to amyloid-β. *J. Am. Chem. Soc.* **2013**, *135*, 10810−10816.
(27) Sheldrick, G. M. *SADABS, Program for Empirical Absorption Correction of Area Detector Data*; University of Gottingen: Gottingen, Germany, 1996.
(28) Sheldrick, G. M. *SHELXL-97 Program for the Refinement of Crystal Structure from Diffraction Data*; University of Gottingen: Gottingen, Germany, 1997.
(29) Cui, M.; Ono, M.; Kimura, H.; Liu, B.; Saji, H. Synthesis and structure−affinity relationships of novel dibenzylideneacetone derivatives as probes for β-amyloid plaques. *J. Med. Chem.* **2011**, *54*, 2225−2240.
(30) Yang, Y.; Cui, M.; Jin, B.; Wang, X.; Li, Z.; Yu, P.; Jia, J.; Fu, H.; Jia, H.; Liu, B. ^{99m}Tc-labeled dibenzylideneacetone derivatives as potential SPECT probes for in vivo imaging of β-amyloid plaque. *Eur. J. Med. Chem.* **2013**, *64*, 90−98.
(31) Becke, A. D. Density-functional thermochemistry. III. The role of exact exchange. *J. Chem. Phys.* **1993**, *98*, 5648−5652.
(32) Stephens, P. J.; Devlin, F. J.; Chabalowski, C. F.; Frisch, M. J. Ab initio calculation of vibrational absorption and circular dichroism spectra using density functional force fields. *J. Chem. Phys.* **1994**, *98*, 11623−11627.
(33) Dobbs, K. D.; Hehre, W. J. Molecular orbital theory of the properties of inorganic and organometallic compounds. 6. Extended basis sets for second-row transition metals. *J. Comput. Chem.* **1987**, *8*, 880−893.
(34) Hehre, W. J.; Ditchfield, R.; Pople, J. A. Self-consistent molecular orbital methods. XII. Further extensions of Gaussian-type basis sets for use in molecular orbital studies of organic molecules. *J. Chem. Phys.* **1972**, *56*, 2257−2261.
(35) Frisch, M. J.; Trucks, G. W.; Schlegel, H. B.; Scuseria, G. E.; Robb, M. A.; Cheeseman, J. R.; Scalmani, G.; Barone, V.; Mennucci, B.; Petersson, G. A.; Nakatsuji, H.; Caricato, M.; Li, X.; Hratchian, H. P.; Izmaylov, A. F.; Bloino, J.; Zheng, G.; Sonnenberg, J. L.; Hada, M.; Ehara, M.; Toyota, K.; Fukuda, R.; Hasegawa, J.; Ishida, M.; Nakajima, T.; Honda, Y.; Kitao, O.; Nakai, H.; Vreven, T.; Montgomery, J. A., Jr.; Peralta, J. E.; Ogliaro, F.; Bearpark, M.; Heyd, J. J.; Brothers, E.; Kudin, K. N.; Staroverov, V. N.; Keith, T.; Kobayashi, R.; Normand, J.; Raghavachari, K.; Rendell, A.; Burant, J. C.; Iyengar, S. S.; Tomasi, J.; Cossi, M.; Rega, N.; Millam, J. M.; Klene, M.; Knox, J. E.; Cross, J. B.; Bakken, V.; Adamo, C.; Jaramillo, J.; Gomperts, R.; Stratmann, R. E.; Yazyev, O.; Austin, A. J.; Cammi, R.; Pomelli, C.; Ochterski, J. W.; Martin, R. L.; Morokuma, K.; Zakrzewski, V. G.; Voth, G. A.; Salvador, P.; Dannenberg, J. J.; Dapprich, S.; Daniels, A. D.; Farkas, O.; Foresman, J. B.; Ortiz, J. V.; Cioslowski, J.; Fox, D. J. *Gaussian 09*, Revision B.01; Gaussian, Inc.: Wallingford CT, 2010.
(36) Humphrey, W.; Dalke, A.; Schulten, K. VMD: Visual molecular dynamics. *J. Mol. Graph.* **1996**, *14*, 33−38.
(37) *Sybyl-X*, version 1.1; Tripos Inc.: St. Louis, MO, 2010.
(38) Zeng, H.; Zhang, H. Combined 3D-QSAR modeling and molecular docking study on 1,4-dihydroindeno[1,2-*c*]pyrazoles as VEGFR-2 kinase inhibitors. *J. Mol. Graphics Modell.* **2010**, *29*, 54−71.
(39) Morris, G. M.; Goodsell, D. S.; Halliday, R. S.; Huey, R.; Hart, W. E.; Belew, R. K.; Olson, A. J. Automated docking using a lamarckian genetic algorithm and an empirical binding free energy function. *J. Comput. Chem.* **1998**, *19*, 1639−1662.
(40) Huey, R.; Morris, G. M.; Olson, A. J.; Goodsell, D. S. A semiempirical free energy force field with charge-based desolvation. *J. Comput. Chem.* **2007**, *28*, 1145−1152.
(41) Huey, R.; Goodsell, D. S.; Morris, G. M.; Olson, A. J. Grid-based hydrogen bond potentials with improved directionality. *Lett. Drug Des. Discovery* **2004**, *1*, 178−183.
(42) Petkova, A. T.; Yau, W.-M.; Tycko, R. Experimental constraints on quaternary structure in alzheimer's β-amyloid fibrils. *Biochemistry* **2005**, *45*, 498−512.
(43) Gasteiger, J.; Marsili, M. Iterative partial equalization of orbital electronegativity—a rapid access to atomic charges. *Tetrahedron* **1980**, *36*, 3219−3228.
(44) Morris, G. M.; Huey, R.; Lindstrom, W.; Sanner, M. F.; Belew, R. K.; Goodsell, D. S.; Olson, A. J. AutoDock4 and AutoDockTools4: automated docking with selective receptor flexibility. *J. Comput. Chem.* **2009**, *30*, 2785−2791.
(45) Raghavan, S.; Rajender, A. Target alcohol/phenol release by cyclative cleavage using glycine as a safety catch linker. *Chem. Commun.* **2002**, 1572−1573.
(46) Abe, Y.; Aoki, T.; Jia, H.; Hadano, S.; Namikoshi, T.; Kakihana, Y.; Liu, L.; Zang, Y.; Teraguchi, M.; Kaneko, T. Chiral Teleinduction in Asymmetric Polymerization of 3,5-Bis(hydroxymethyl)phenylacetylene Having a Chiral Group via a Very Long and Rigid Spacer at 4-Position. *Chem. Lett.* **2012**, *41*, 244−246.
(47) Kimball, F. S.; Romero, F. A.; Ezzili, C.; Garfunkle, J.; Rayl, T. J.; Hochstatter, D. G.; Hwang, I.; Bogeret, D. L. Optimization of α-Ketooxazole Inhibitors of Fatty Acid Amide Hydrolase. *J. Med. Chem.* **2008**, *51*, 937−947.
(48) Ma, L.; Morgan, J. C.; Stancill, W. E.; Allen, W. E. Phosphorylated 1,6-diphenyl-1,3,5-hexatriene. *Bioorg. Med. Chem. Lett.* **2004**, *14*, 1075−1078.
(49) Oriyama, T.; Noda, K.; Yatabe, K. Highly Efficient and Convenient Methods for the Direct Conversion of Aryl Silyl Ethers and Aryl Acetates into Aryl Alkyl Ethers. *Synlett* **1997**, 710−703.